UCRL-ID-143170

Ternary Phase Diagrams that Relate to the Plutonium Immobilization Ceramic

B. B. Ebbinghaus and O. H. Krikorian
Lawrence Livermore National Laboratory

E. R. Vance and M. W. Stewart
Autralian Nuclear Science and Technology Organisation

U.S. Department of Energy
Lawrence Livermore National Laboratory

January 1, 2001

DISCLAIMER

This document was prepared as an account of work sponsored by an agency of the United States Government. Neither the United States Government nor the University of California nor any of their employees, makes any warranty, express or implied, or assumes any legal liability or responsibility for the accuracy, completeness, or usefulness of any information, apparatus, product, or process disclosed, or represents that its use would not infringe privately owned rights. Reference herein to any specific commercial product, process, or service by trade name, trademark, manufacturer, or otherwise, does not necessarily constitute or imply its endorsement, recommendation, or favoring by the United States Government or the University of California. The views and opinions of authors expressed herein do not necessarily state or reflect those of the United States Government or the University of California, and shall not be used for advertising or product endorsement purposes.

This work was performed under the auspices of the U. S. Department of Energy by the University of California, Lawrence Livermore National Laboratory under Contract No. W-7405-Eng-48.

This report has been reproduced directly from the best available copy.

Available electronically at http://www.doc.gov/bridge

Available for a processing fee to U.S. Department of Energy
And its contractors in paper from
U.S. Department of Energy
Office of Scientific and Technical Information
P.O. Box 62
Oak Ridge, TN 37831-0062
Telephone: (865) 576-8401
Facsimile: (865) 576-5728
E-mail: reports@adonis.osti.gov

Available for the sale to the public from
U.S. Department of Commerce
National Technical Information Service
5285 Port Royal Road
Springfield, VA 22161
Telephone: (800) 553-6847
Facsimile: (703) 605-6900
E-mail: orders@ntis.fedworld.gov
Online ordering: http://www.ntis.gov/ordering.htm

OR

Lawrence Livermore National Laboratory
Technical Information Department's Digital Library
http://www.llnl.gov/tid/Library.html

Abstract

The plutonium immobilization ceramic consists primarily of a pyrochlore titanate phase of the approximate composition $Ca_{0.97}Hf_{0.17}Pu_{0.22}U_{0.39}Gd_{0.24}\ Ti_2O_7$. In this study, a series of ternary phase diagrams was constructed to evaluate the relationship of various titanate phases (e.g., brannerite, zirconolite-2M, zirconolite-4M, and perovskite) to pyrochlore titanates, usually in the presence of excess TiO_2 (rutile), and at temperatures in the vicinity of 1350°C. To facilitate the studies, U, Th, and Ce were used as surrogates for Pu in a number of the phase diagrams in addition to the use of Pu itself. The effects of impurity oxides, Al_2O_3 and MgO, were also studied on pyrochlore ($Gd_2Ti_2O_7$) and zirconolite ($CaHfTi_2O_7$) mixtures. Either electron microprobe (at Lawrence Livermore National Laboratory) or quantitative SEM-EDS (at Australian Nuclear Science and Technology Organisation) were used to evaluate the compositions of the phases.

Introduction

The purpose of this report is to show the relationships of the mineral phases in the plutonium immobilization ceramic [1] at or near the temperature of preparation. As envisioned at the time of preparation of the samples for these phase studies, the target mineralogy and phase composition of the ceramic immobilization form (original baseline formulation) was:

95.0 wt % pyrochlore ($Ca_{0.890}Hf_{0.230}Pu_{0.220}U_{0.440}Gd_{0.220}Ti_2 0_7$)

5.0 wt % rutile ($Ti_{0.913}Hf_{0.087}O_2$)

In practice, the target composition would form as primarily pyrochlore, with about 10 vol% brannerite, 10 vol% rutile, small amounts of zirconolite, and trace amounts of actinide oxide. Addition of impurities would alter the percentages of the minerals and could introduce small amounts of other minerals. Also the temperature of preparation and oxidizing or reducing conditions could affect the mineralogy.

In this report, the mineral compositions are given for a number of ternary systems using U, Th, or Ce as surrogates for Pu, as well as Pu itself, with a variation of compositions intended to show the mineral behavior with departures from the baseline formulation. Preparation temperatures are at or near 1350°C, and preparations are either in air, Ar, or in some cases reduced oxygen pressures. For samples prepared by the authors (P series and ME series), the methods of preparation are described in separate reports for the P series [2] and for the ME series [3]. References are cited for other samples used. In addition to the ternary phase diagrams given here, ternary phase diagrams for compositions in which Ce is used as a surrogate for Pu and U, are given in a separate report [4].

Phase Diagram Determinations

Samples prepared for phase diagram determinations at the Lawrence Livermore National Laboratory (LLNL) were usually first analyzed by x-ray diffraction to identify the bulk mineral phases and then by electron microprobe to establish the atomic compositions of the phases. The electron microprobe results are summarized in **Appendix A**. A large number of samples prepared by the Australian Nuclear Science and Technology Organisation (ANSTO) are also used for the phase diagram determinations. The analyses of the ANSTO samples were obtained by quantitative SEM/EDS and their data are also listed in **Appendix A**. When combined LLNL and ANSTO data are included in a phase diagram, the LLNL data are indicated by (L) in the figure legend and the ANSTO data by (A). Abbreviations used for the phases in the diagrams are R for rutile, Pv for perovskite, Br for brannerite, Py for pyrochlore, Z-2M for zirconolite-2M, Z-3O for zirconolite-3O, Z-4M for zirconolite-4M, HT for hafnium titanate, AT for aluminum titanate (otherwise known as pseudobrookite), MT for magnesium titanate (otherwise known as armalcolite), U for uranium oxide, T for thorium oxide, and P for plutonium oxide. Usually the TiO_2 content and in some cases the CaO content are not plotted in the phase diagrams in order to allow depiction of the phase diagrams by a ternary representation. TiO_2 and CaO contents can be obtained for the desired compositions by referring to individual data points in **Appendix A**. When TiO_2 contents are not plotted on the diagrams, the TiO_2 is present in excess for the phases that are formed. The preparation temperatures of the individual samples are not always at the indicated temperature of the phase diagram but may vary up to 100°C above or below the indicated temperature. This should not significantly affect the phase diagram if phase changes do not occur. For phase diagrams determined in an Ar atmosphere, the Ar was not maintained at high purity in the furnace atmosphere, and O_2 and H_2O levels of 50-100 ppm are expected to have been present.

$Gd_2Ti_2O_7$-$CaHfTi_2O_7$-Al_2TiO_5 Phase Diagram at 1400°C in Air

The $Gd_2Ti_2O_7$-$CaHfTi_2O_7$-Al_2TiO_5 phase diagram at 1400°C in air (see **Figure 1**) was studied in the excess TiO_2 region to determine the effects of Al_2O_3 on the pyrochlore ($Gd_2Ti_2O_7$), zirconolite-2M ($CaHfTi_2O_7$), and a zirconolite-4M phase that occur in the $Gd_2Ti_2O_7$-$CaHfTi_2O_7$ binary system. A single phase sample of Hf-substituted zirconolite-2M, $CaHfTi_2O_7$, of ~99 % purity was prepared and characterized by SEM/EDS at ANSTO [5]. Analytic data on other samples prepared in the ternary system are listed in **Appendix A** for LLNL samples SM0623a to SM1116b, and ANSTO samples mws980401 to mws980425, L990657 to L990675, L990820 to L990824, and mws990495. There is an extensive solid solution range for the zirconolite-2M phase although the alumina-rich boundary was not established with the samples that were studied. Zirconolite-4M shows only a slight solid solution extension with added alumina. However, a new phase with a large alumina content forms within the ternary diagram. X-ray diffraction data [6,7] show only zirconolite type patterns in this region, but patterns that are

different than those for zirconolite-2M and zirconolite-4M. From work conducted at ANSTO, this phase has been identified as zirconolite-3O [8]. Solubility of $AlO_{1.5}$ in pyrochlore is about 5 mol %. The hafnia content of the rutile averages 9 mol % in these samples with low solubilities of other constituents. This system shows that alumina is a strong zirconolite stabilizer.

$Gd_2Ti_2O_7$-$CaHfTi_2O_7$-$MgTi_2O_5$ Phase Diagram at 1400°C in Air

The $Gd_2Ti_2O_7$-$CaHfTi_2O_7$-$MgTi_2O_5$ phase diagram at 1400°C in air (see **Figure 2**) in the presence of excess TiO_2 was studied to determine the effects of MgO on the pyrochlore and zirconolite phases. Binary $Gd_2Ti_2O_7$-$CaHfTi_2O_7$ data are given above for the alumina system. Data within the ternary system here are listed in **Appendix A** as samples L990662 to L990694, L990815 to L990819, and mws990491. The solubility of MgO in the zirconolite-2M phase is extensive although the limit was not established. Solubility of MgO in zirconolite-4M is low. A zirconolite phase with a large homogeneity range forms within the ternary system. X-ray diffraction patterns for this phase [6,7] are similar to those for the phase labeled as zirconolite-3O in the alumina system. Solubility of MgO in the pyrochlore phase is about 10-15 mol %. The hafnia content of rutile averages about 6 mol % in these samples. As was the case with the alumina system, MgO is a strong zirconolite stabilizer, although it shows a fairly high solubility in pyrochlore as well.

TiO_2-CaO-U_3O_{8-x} Phase Diagram at 1350°C in Air

The TiO_2-CaO-U_3O_{8-x} phase diagram at 1350°C in air is given in **Figure 3**. Data on this system comes primarily from ANSTO (see samples R00m026 (90% UTi_2O_6 + 10% $CaTiO_3$) to R00m026 (90% $CaUTi_2O_7$ + 10% $CaTiO_3$) in **Appendix A**), where it was found that although uranium brannerite does not form in the U_3O_{8-x}-TiO_2 binary system in air, the addition of CaO stabilizes the phase. The pyrochlore phase composition was found to be shifted to a higher Ca and lower U content than in stoichiometric $CaUTi_2O_7$. Solubilities of U and Ca oxides in rutile were found to be low. Some LLNL samples containing small amounts of HfO_2 (see samples P262, P266, and P270 in **Appendix A**) provided additional information on brannerite and pyrochlore compositions, and one data point for perovskite and three data points for rutile. One of the rutile data points agreed with the ANSTO data, but two of the data points indicated anomolously high solubilities for Ca and U oxides and are rejected. No information was obtained for the high Ca and U oxide regions of the phase diagram, but U oxide is assumed to exist as U_3O_{8-x} [9], and a mixed oxide $Ca_2UO_{4.37}$ [10] also seems likely.

Figure 1. $Gd_2Ti_2O_7$-$CaHfTi_2O_7$-Al_2TiO_5 phase diagram at 1400°C in air.

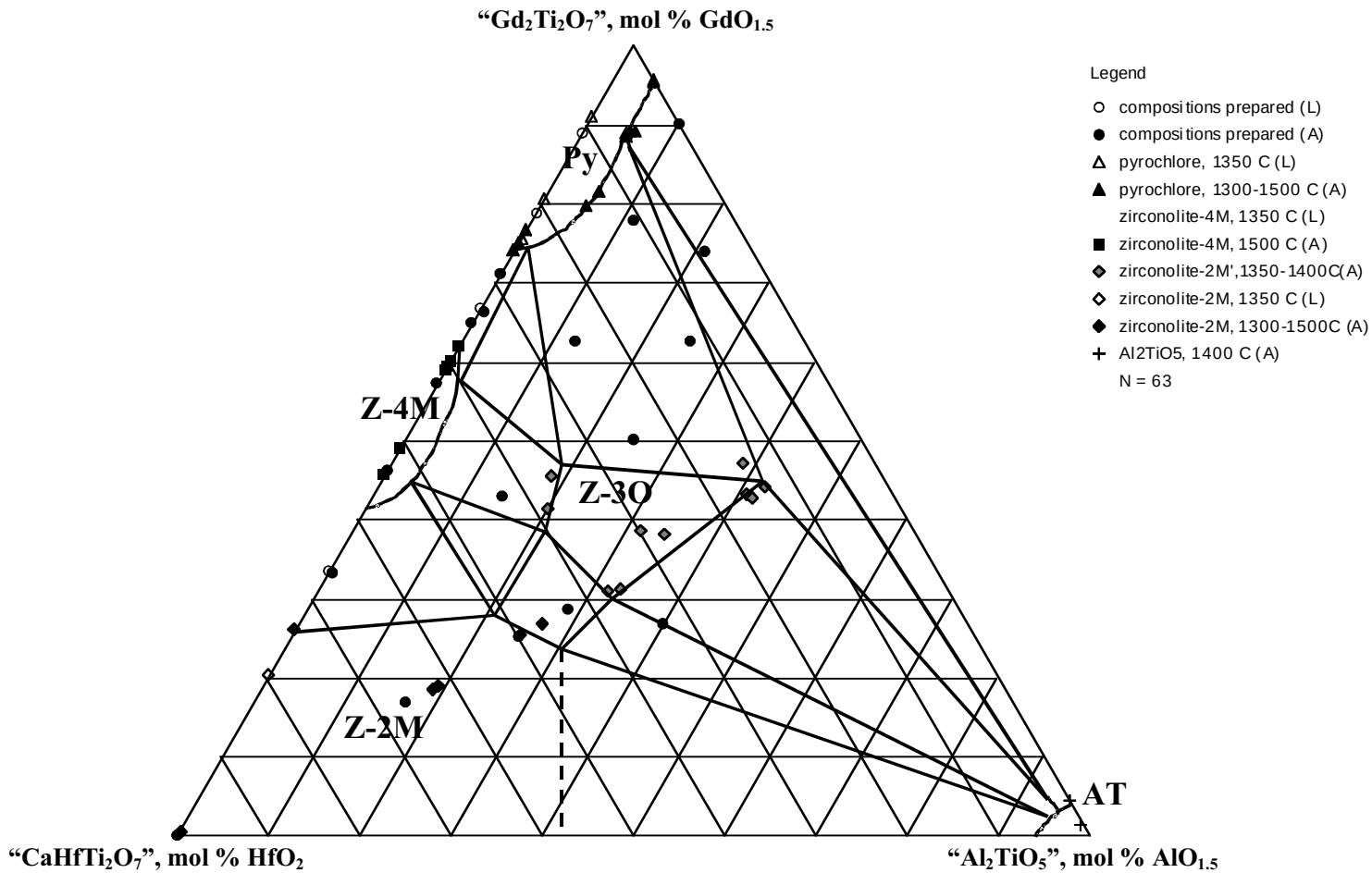

Figure 2. $Gd_2Ti_2O_7$-$CaHfTi_2O_7$-$MgTi_2O_5$ phase diagram at 1400ºC in air.

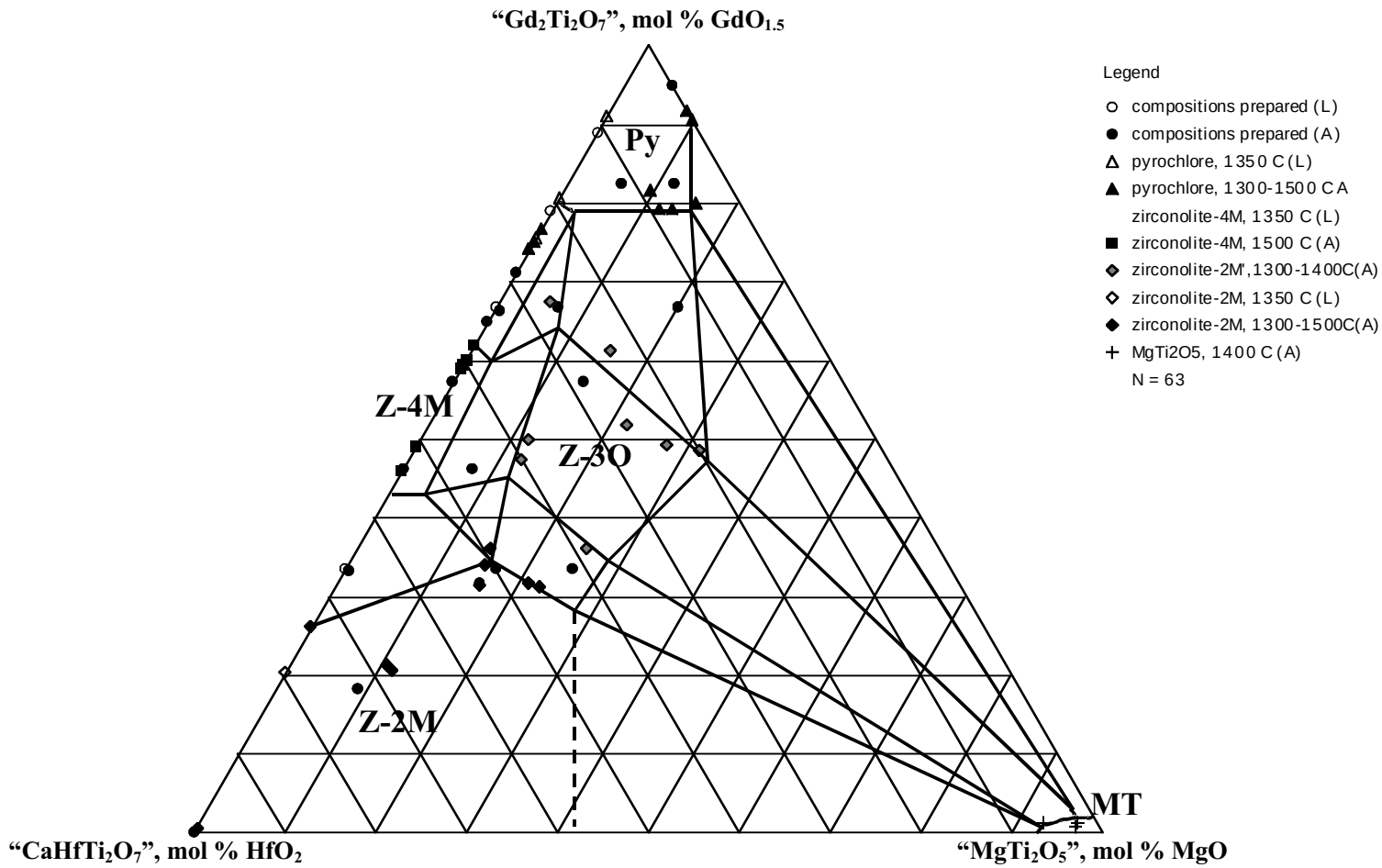

Figure 3. TiO_2-CaO-U_3O_{8-x} phase diagram at 1350°C in air.

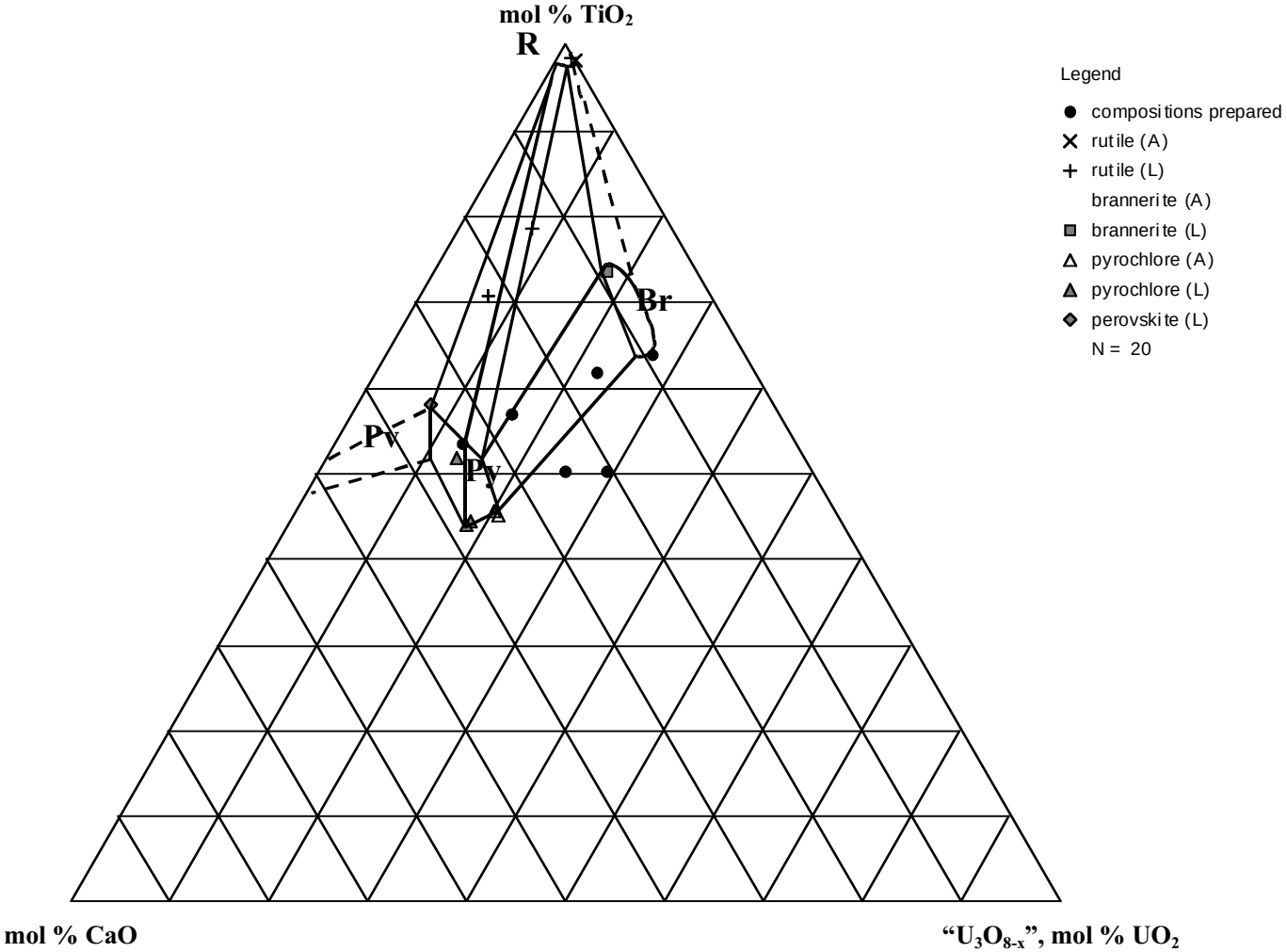

TiO_2-CaO-UO_2 Phase Diagram at 1350°C in Ar

The TiO_2-CaO-UO_2 phase diagram at 1350°C in Ar (see **Figure 4**) is based upon LLNL samples P199A through P287 in **Appendix A**. In addition, a preparation of uranium brannerite (P254) was made in the binary UO_2-TiO_2 system. This preparation was made by heating a powder mixture of UO_2 and TiO_2 at 1350°C in a 5%CO/95%CO_2 atmosphere for 300 hours. The heating was stopped periodically during the run and the sample was checked by X-ray diffraction to determine the extent of reaction. Then the sample was ground finer and returned to the heating. After 300 hours, the reaction appeared to be complete. There was no rutile present, but there was a trace of UO_2, which was estimated from the X-ray intensity to be about 0.3 mole %. The makeup mixture of the sample gave it a composition of $U_{0.952}Ti_{2.048}O_6$, and this is shown as a "composition prepared" on the phase diagram. Some of the prepared sample of $U_{0.952}Ti_{2.048}O_6$ was pressed into a pellet and reheated at 1350°C for 48 hours in 5%CO/95%CO_2. SEM analysis showed about 30 % decompostion of the brannerite into rutile and UO_2. Therefore, CaO-free uranium brannerite is only marginally stable at 1350°C in a low O_2 atmosphere. The high CaO limit of the brannerite is similar to that in the air phase diagram, and the pyrochlore and rutile compositions are also similar to the air phase diagram. Perovskite shows a lower solubility for UO_2 than in the air phase diagram. A mixed oxide "CaU_2O_5" is found to coexist with the pyrochlore and brannerite phases.

$CaTiO_3$-$HfTiO_4$-$UTi_2O_{6.5}$ Phase Diagram at 1350°C in Air

The $CaTiO_3$-$HfTiO_4$-$UTi_2O_{6.5}$ phase diagram at 1350°C in air is shown in **Figure 5**. Data are from LLNL samples P259 through P270 and the first two ANSTO R00m026 samples given earlier (see **Appendix A**). U is assumed to have a valence of +5 for samples in air at 1350°C, hence brannerite has the formula $UTi_2O_{6.5}$. The $CaTiO_3$-$UTi_2O_{6.5}$ binary in this diagram is a rutile-rich projection from the TiO_2-CaO-U_3O_{8-x} phase diagram given above, and the rest of the phase diagram is also in the rutile-rich region. The electron microprobe data for the zirconolite phase is taken to be all for zirconolite-2M because there is no X-ray diffraction evidence for zirconolite-4M in the samples for this region, hence the zirconolite-2M phase extends over a wide range. Hafnium titanate coexists with brannerite, pyrochlore and zirconolite-2M. Solubilities of Hf and U oxides in perovskite are sporadic with one sample showing a very low solubility and three samples showing high solubilities. A low HfO_2 solubility was chosen here since some of the other ternary systems studied in this work indicate a low HfO_2 solubility in $CaTiO_3$. Conversely, a relatively high solubility is taken for U oxide in $CaTiO_3$. Rutile compositions also showed a high variability in these samples. Hafnia content averaged 6 mol %, urania content 3 mol % and calcia content ranged from 0 to 22 mol %.

.

Figure 4. TiO_2-CaO-UO_2 phase diagram at 1350°C in Ar.

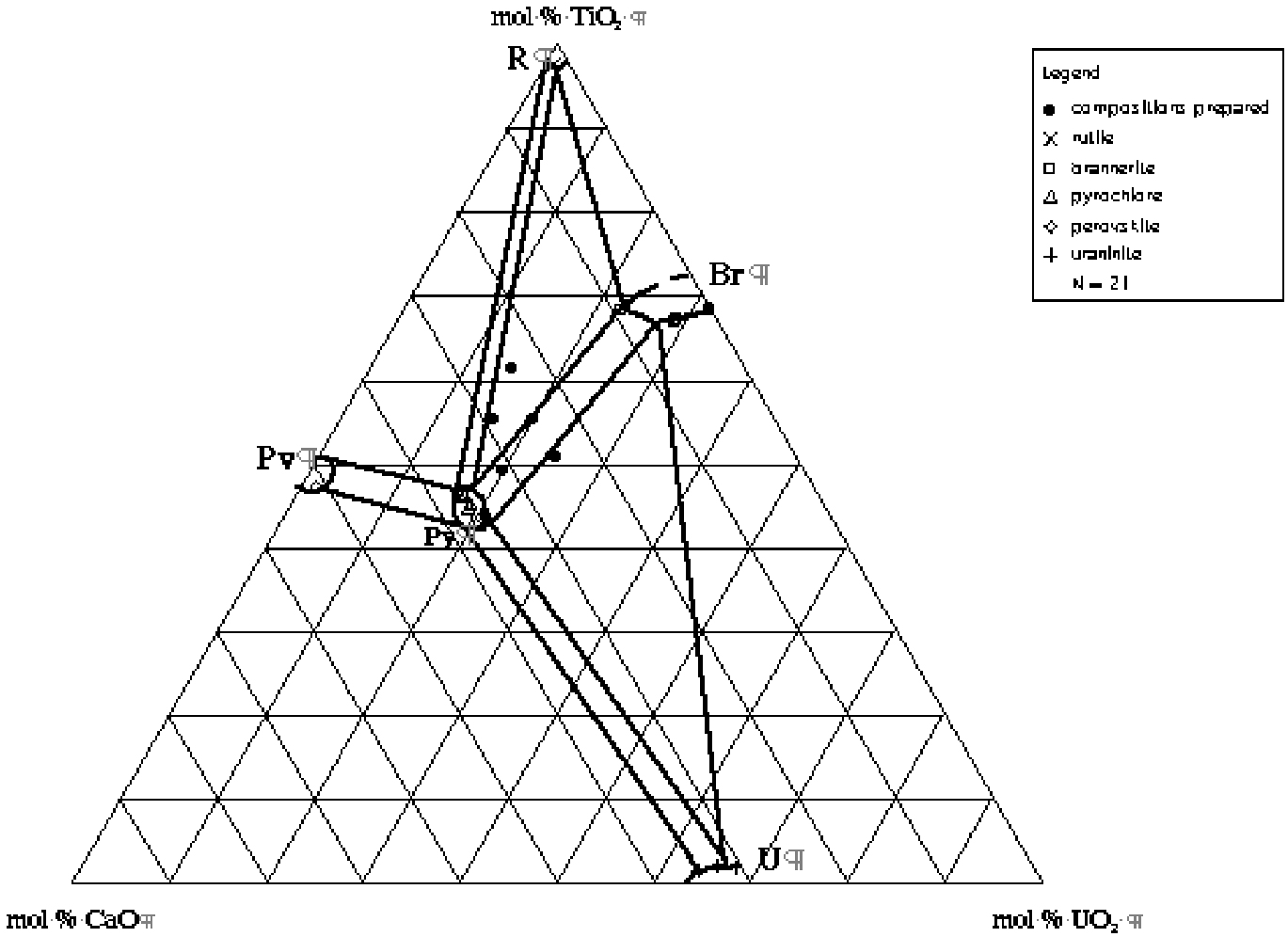

Figure 5. $CaTiO_3$-$HfTiO_4$-$UTi_2O_{6.5}$ phase diagram at 1350°C in air.

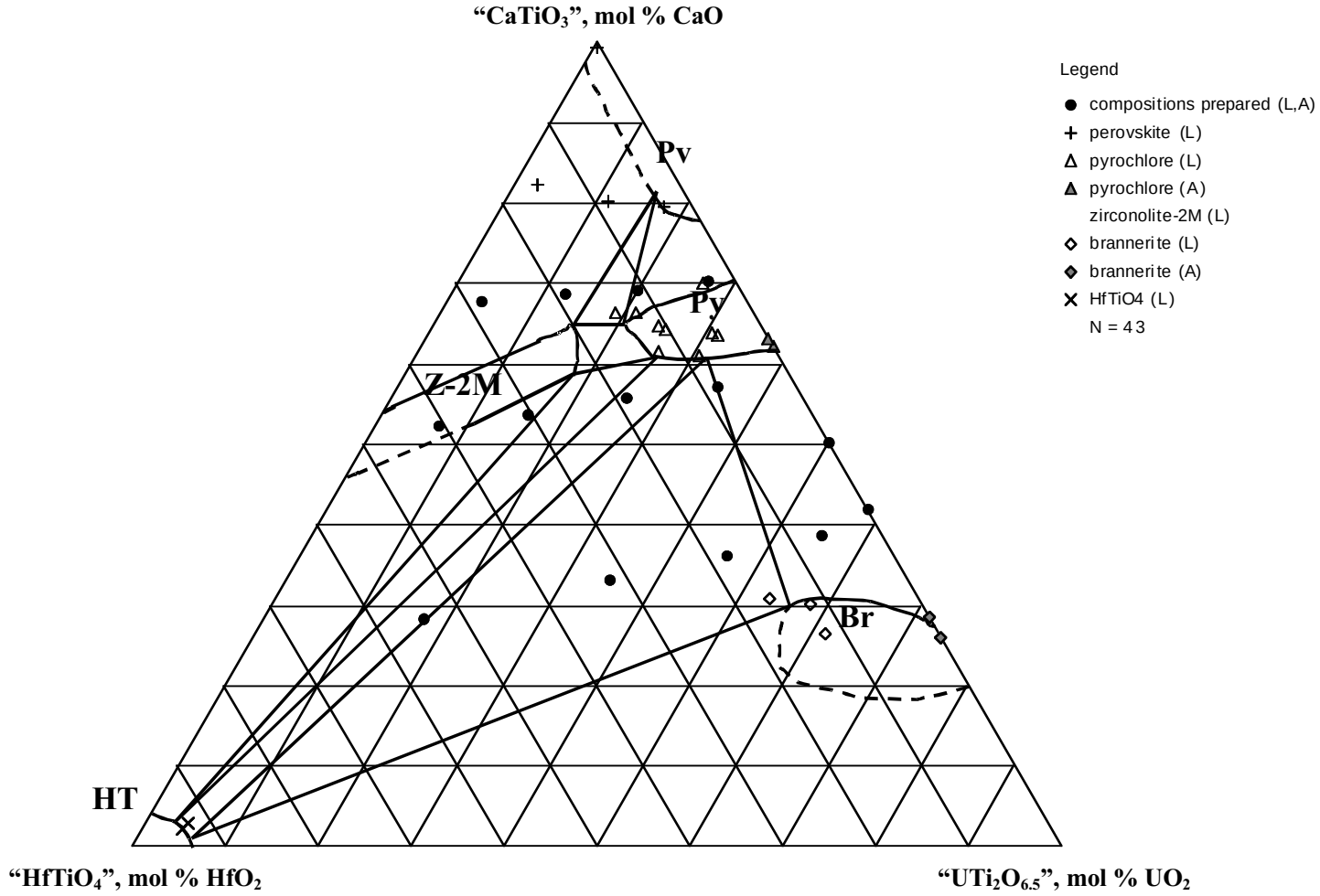

$CaTiO_3$-$HfTiO_4$-UTi_2O_6 Phase Diagram at 1350°C in Ar

The $CaTiO_3$-$HfTiO_4$-UTi_2O_6 phase diagram at 1350°C in Ar (see **Figure 6**) presents a projection of the high rutile region of **Figure 4** from brannerite to perovskite, and also represents high rutile for the balance of the diagram with the $HfTiO_4$ additions. Samples L990357 – L990369 from ANSTO (see **Appendix A**) cover the bulk of the diagram while earlier LLNL samples P201A, P249, P250 and P287 (in **Appendix A**) cover the $CaTiO_3$-UTi_2O_6 binary region. Comparing with the phase diagram in air, the brannerite phase in Ar is extended to CaO-free UTi_2O_6 and the UO_2 content in brannerite is lowered within the ternary system. UO_2 contents in pyrochlore and zirconolite-2M are increased within the ternary system relative to the phase diagram in air, and perovskite shows a low solubility for UO_2. Hafnia content of the rutile is about 12 mol %.

$Gd_2Ti_2O_7$-$Ca_{1.45}U_{0.65}Ti_{1.9}O_{6.9}$-$CaHfTi_2O_7$ Phase Diagram at 1350°C in Air

The $Gd_2Ti_2O_7$-$Ca_{1.45}U_{0.65}Ti_{1.9}O_{6.9}$-$CaHfTi_2O_7$ phase diagram at 1350°C in air (see **Figure 7**) studies the effect of $Gd_2Ti_2O_7$ additions on a section through the pyrochlore and zirconolite-2M phases shown in **Figure 5**. LLNL samples are SM0623a, SM1116b, P260, P261, P264, P265 and P267, and ANSTO samples are mws980401 – mws980425 (all given earlier), and new LLNL samples are P285 – P292 (all in **Appendix A**). Zirconolite-4M stabilizes with addition of about 5 mole % $Gd_2Ti_2O_7$ (10 mole % $GdO_{1.5}$ on the diagram), and the three phases advance uniformly to the $Gd_2Ti_2O_7$-$CaHfTi_2O_7$ binary. The hafnia content of rutile averages 10 mol % and calcia and urania contents are generally on the order of a few mol %

.

Figure 6. $CaTiO_3$-$HfTiO_4$-UTi_2O_6 phase diagram at 1400°C in Ar.

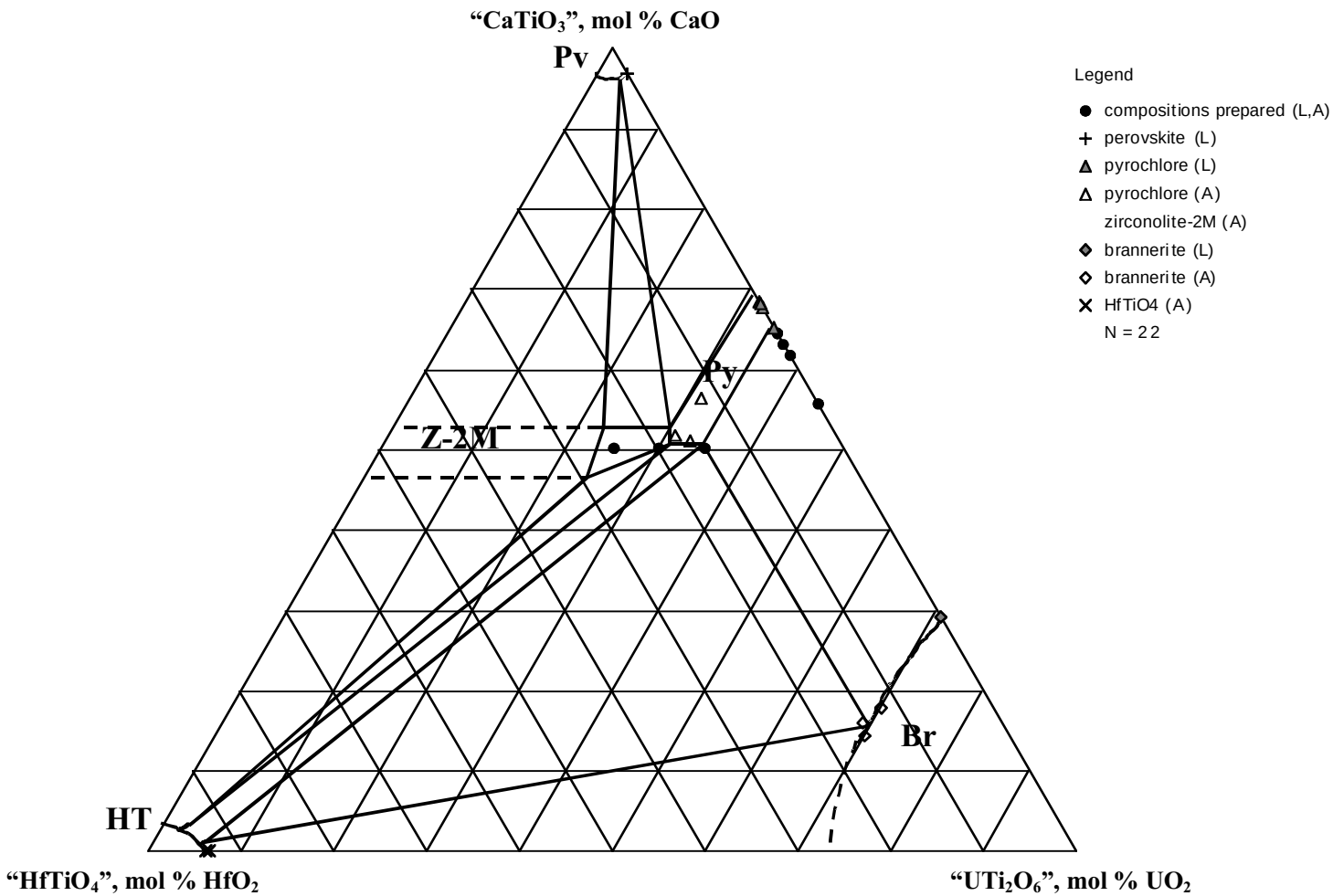

Figure 7. $Gd_2Ti_2O_7$-$Ca_{1.45}U_{0.65}Ti_{1.9}O_{6.9}$-$CaHfTi_2O_7$ phase diagram at 1350°C in air.

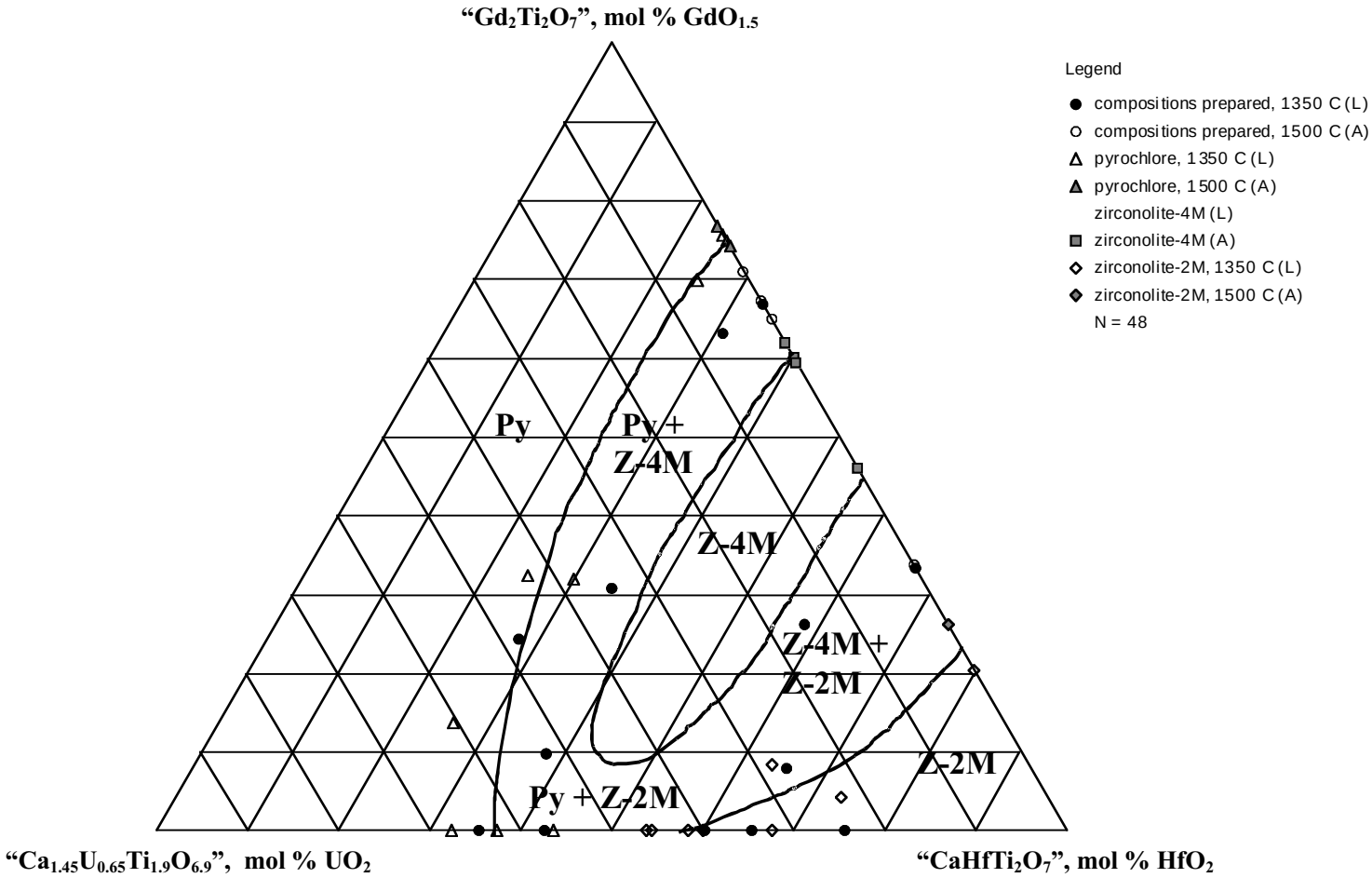

$Gd_2Ti_2O_7$-$Ca_{1.46}U_{0.69}Ti_{1.85}O_{6.54}$-$CaHfTi_2O_7$ Phase Diagram at 1400°C in Ar

The $Gd_2Ti_2O_7$-$Ca_{1.46}U_{0.69}Ti_{1.85}O_{6.54}$-$CaHfTi_2O_7$ phase diagram at 1400°C in Ar (see **Figure 8**) represents $Gd_2Ti_2O_7$ additions to a projection across the pyrochlore and zirconolite –2M phases shown in **Figure 6**. The interception of the pyrochlore and zirconolite phases with the $Gd_2Ti_2O_7$-$CaHfTi_2O_7$ binary is taken to be identical with **Figure 7** since oxidizing conditions should not affect these phases. Samples are available from ANSTO as L990357 – L990369 (given earlier) and L990354 – L990368 in **Appendix A** for the bulk of the diagram. The stabilization of zirconolite-4M in this diagram requires a larger amount of $Gd_2Ti_2O_7$ than in **Figure 7** with the air atmosphere. The hafnia content of rutile averages 11 mol %, and the urania content averages less than 1 mol %.

$CaTiO_3$-$HfTiO_4$-$AnTi_2O_6$ Phase Diagram at 1350°C in Ar, An = U + Ce + Gd

This phase diagram (**Figure 9**) represents the behavior of a baseline formulation at 1350°C in Ar. Ce is used as a surrogate for Pu, and An (actinide) is taken as the sum of U + Ce + Gd for plotting purposes. Samples are available from ANSTO (see R97m030-3B to R97m030-8B in **Appendix A**) but contain impurities. The main impurity pickup is Ga pickup by zirconolite-2M in sample R97m030-3B, while the other phases show very low levels of impurities. Only the perovskite phase is given in sample R97m030-8B because the sample had a very high level of impurities, but the perovskite phase showed only a low level of impurity pickup. Some samples were also prepared at LLNL at low oxygen fugacities ($10^{-2.60}$ and $10^{-5.05}$ atm). These samples (Ryerson 1/4 to Ryerson 7/5 in **Appendix A**) should give oxidation conditions similar to those in the ANSTO Ar samples. The LLNL samples contained a small amount of Al impurity. The phase diagram (see **Figure 9**) shows a high solubility for An in perovskite, due primarily to Ce which is expected to be in the +3 state in perovskite [4]. Compared to **Figure 6**, where U is the only actinide plotted, the pyrochlore and zirconolite-2M phases here show lower Ca contents, perhaps a result of replacement of Ca by Gd. Brannerite also shows a lower Ca content. Zirconolite-4M phase is not shown in this diagram. ANSTO previously listed a zirconolite phase in the R97m030-3B sample as zirconolite-4M [11], but it is currently believed that it is a compositional variation in the zirconolite-2M phase because the zirconolite-2M phases in the other samples of **Figure 9** appear to be in equilibrium with pyrochlore. These samples average 7 mol % hafnia and 1 mol % urania in the rutile.

Figure 8. $Gd_2Ti_2O_7$-$Ca_{1.46}U_{0.69}Ti_{1.85}O_{6.54}$-$CaHfTi_2O_7$ phase diagram at 1400°C in Ar.

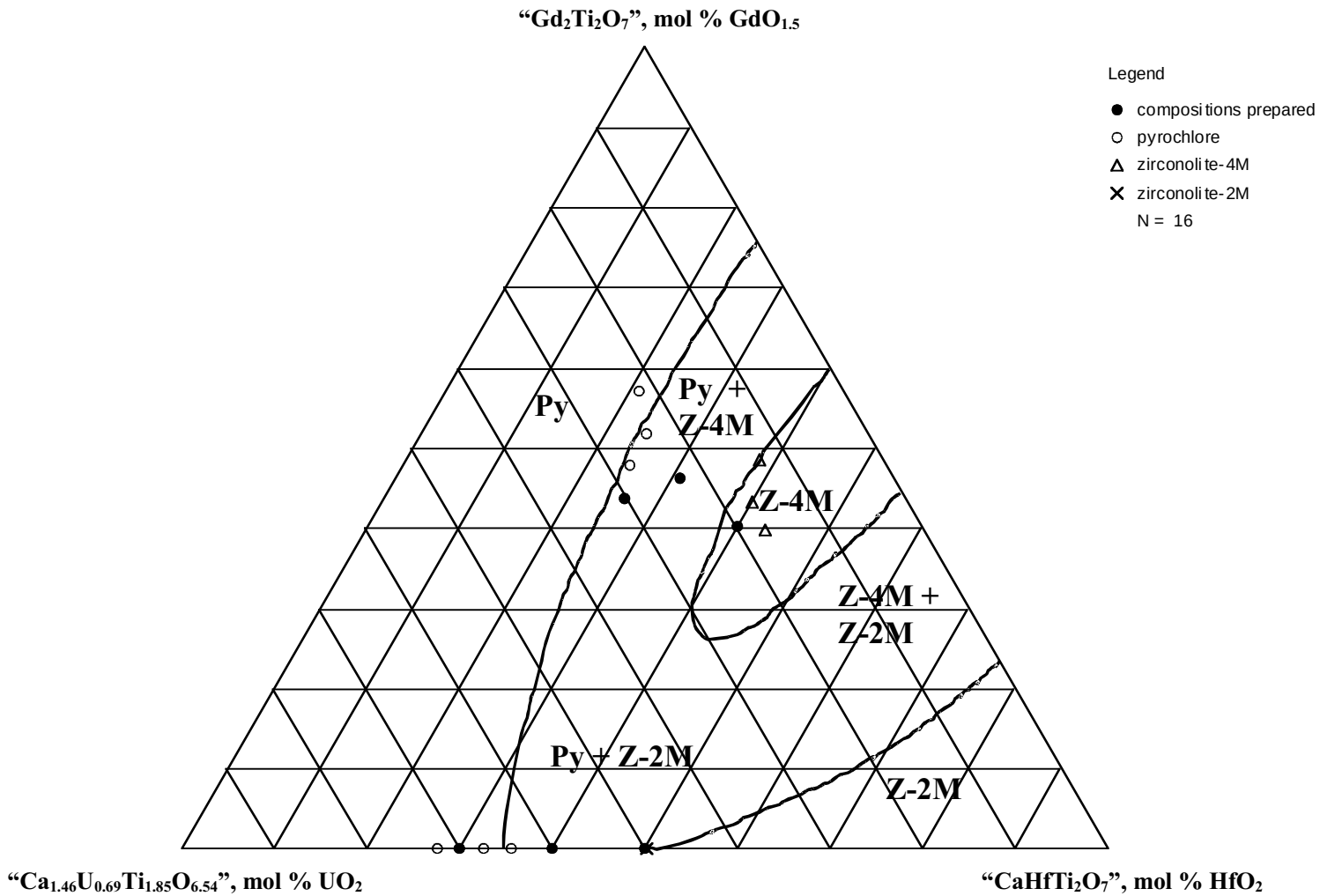

Figure 9. $CaTiO_3$-$HfTiO_4$-$AnTi_2O_6$ phase diagram at 1350ºC in Ar. An = U + Ce + Gd.

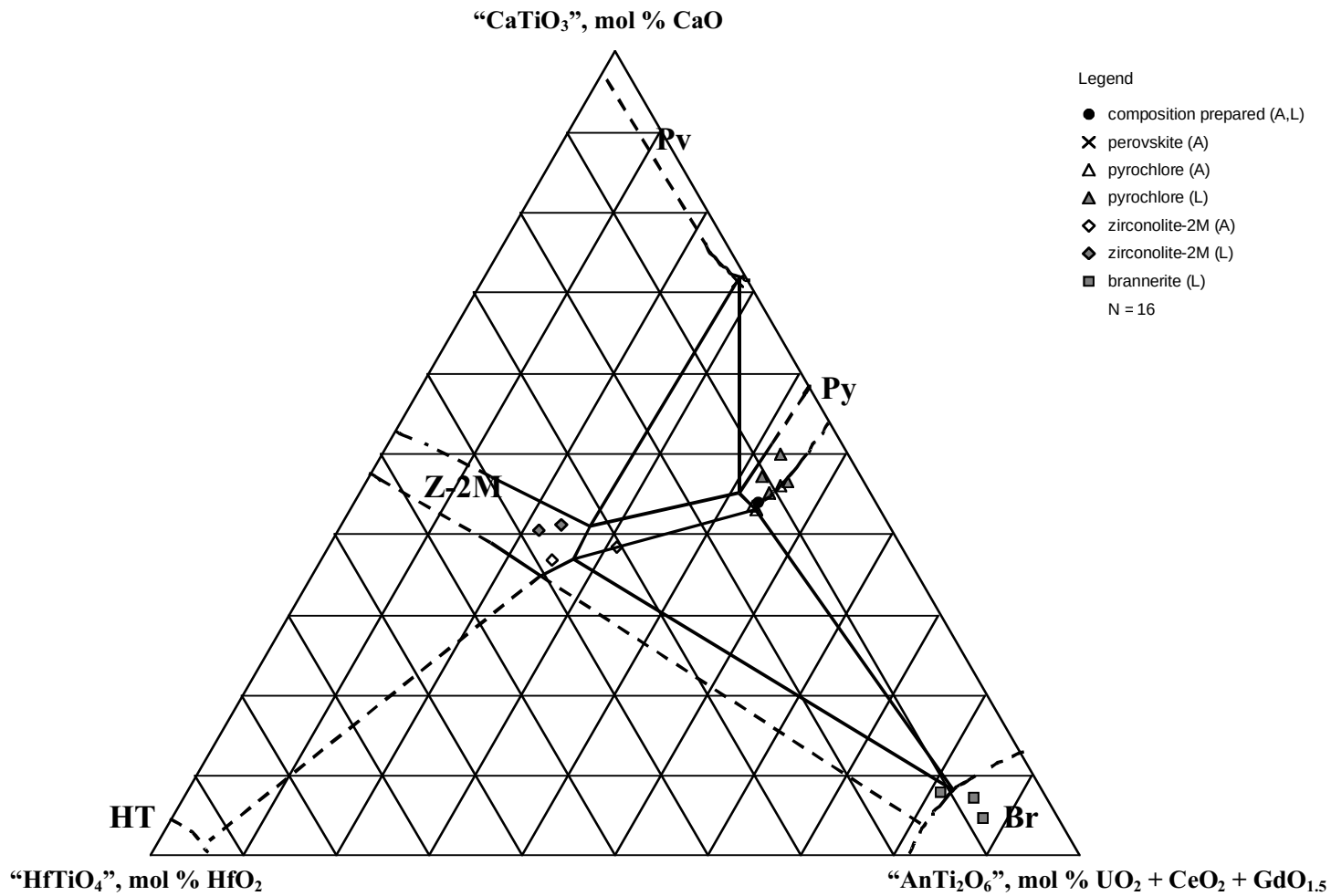

TiO_2-CaO-ThO_2 Phase Diagram at 1350 °C in Air

Begg, et al. [12] from ANSTO report that a Th-pyrochlore does not form in the TiO_2-CaO-ThO_2 system at 1300-1400°C in air (see **Figure 10**). Approximate compositions for brannerite, perovskite, and thoria phases in this phase diagram were taken from the lowest Hf content samples that were prepared for studying the $CaTiO_3$-$HfTiO_4$-$ThTi_2O_6$ phase diagram (see samples L990383, L990389, P301 and P306 in **Appendix A**). The hafnium is assumed to be an inert impurity in determining the compositions in the diagram. The phase diagram is very simple, with some ThO_2 solubility in the perovskite phase and a low CaO solubility in the brannerite phase.

$CaTiO_3$-$HfTiO_4$-$ThTi_2O_6$ Phase Diagram at 1350°C in Air

The $CaTiO_3$-$HfTiO_4$-$ThTi_2O_6$ phase diagram at 1350°C in air is shown in **Figure 11**. Samples from both ANSTO (L990381 – L990389 in **Appendix A**) and LLNL (P300 – P306 in **Appendix A**) were used to construct the phase diagram. The ANSTO data were used primarily to set the solubility limits for the perovskite phase. The zirconolite-2M phase shows an extensive solid solution region, similar to that in the $CaTiO_3$-$HfTiO_4$-$UTi_2O_{6.5}$ system (see **Figure 5**). The pyrochlore phase is stabilized by the presence of HfO_2, but is displaced to a lower CaO content than was the case in the $CaTiO_3$-$HfTiO_4$-$UTi_2O_{6.5}$ system. The solubility of CaO in the brannerite phase shows considerable scatter, indicating a difficulty in establishing equilibrium. A low CaO solubility is selected in view of the low values given by the ANSTO data. Only one compositional point was available for the $HfTiO_4$ phase, and indicated high solubilites for CaO and ThO_2. Hafnia solubility in rutile averages 9 mol %, and there are large variations in the solubilities of calcia and thoria.

$Gd_2Ti_2O_7$-$CaThTi_2O_7$-$CaHfTi_2O_7$ Phase Diagram at 1350°C in Air

The $Gd_2Ti_2O_7$-$CaThTi_2O_7$-$CaHfTi_2O_7$ phase diagram at 1350°C in air (see **Figure 12**) represents $Gd_2Ti_2O_7$ additions to a section across **Figure 11** of the ideal pyrochlore composition, $CaThTi_2O_7$, and zirconolite-2M. Samples for this diagram from ANSTO are listed in Appendix A as L990381 – L990389 and L990378 – L990388, and samples from LLNL are P300 - P306. The phase diagram is similar to that for the U system (see **Figure 7**) in that zirconolite-4M does not exist along the $CaHfTi_2O_7$ - $CaThTi_2O_7$ line, but is stabilized by addition of $Gd_2Ti_2O_7$. The phase boundary intercepts along the $Gd_2Ti_2O_7$ – $CaHfTi_2O_7$ line are taken to be identical to those found for the U system (**Figure 7**). Pyrochlore disproportionates into brannerite and perovskite as the composition, $CaThTi_2O_7$, is approached. Hafnia solubility in rutile is 9 mol % in this system.

Figure 10. TiO_2-CaO-ThO_2 phase diagram at 1350°C in air.

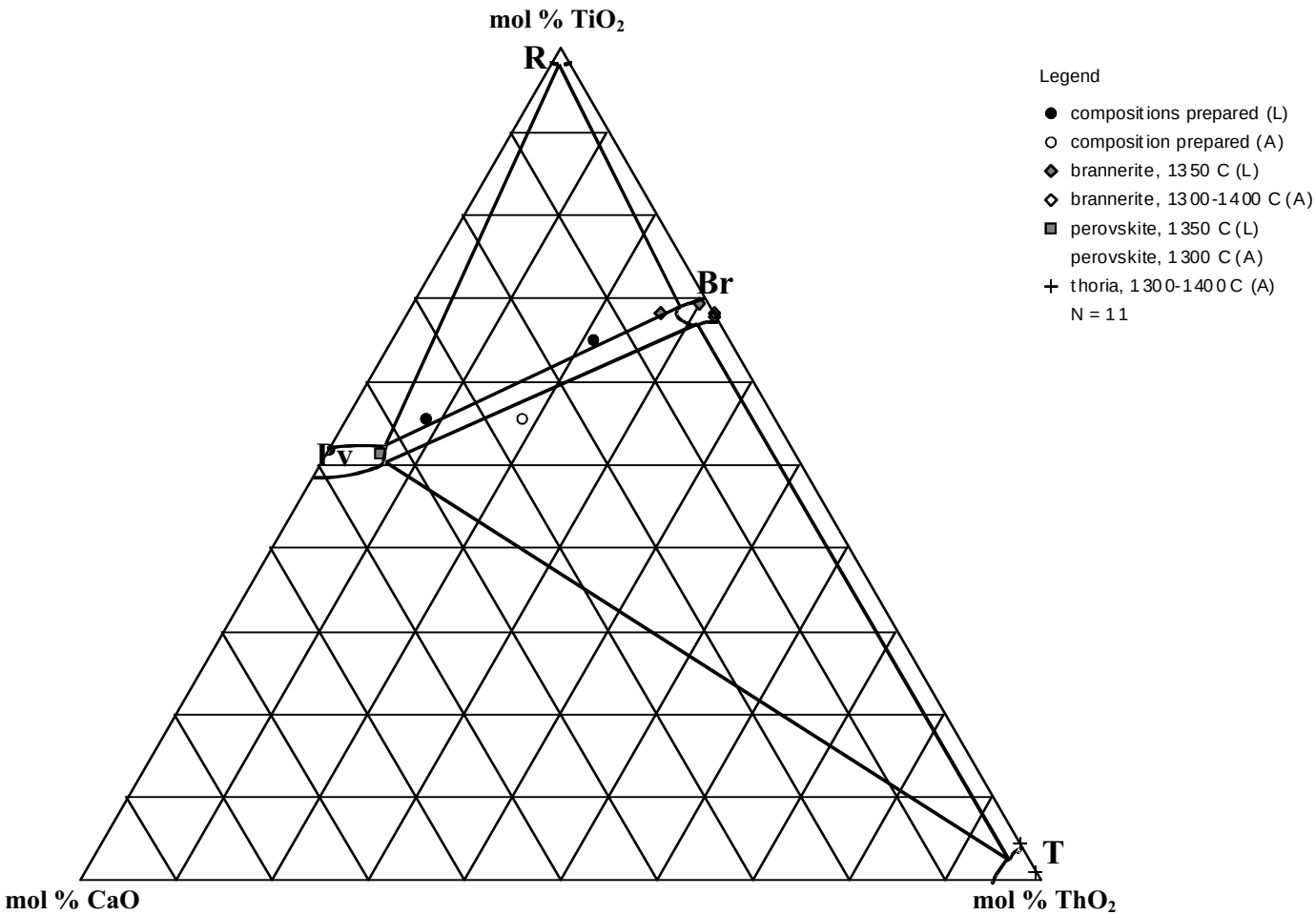

Figure 11. $CaTiO_3$-$HfTiO_4$-$ThTi_2O_6$ phase diagram at 1350ºC in air.

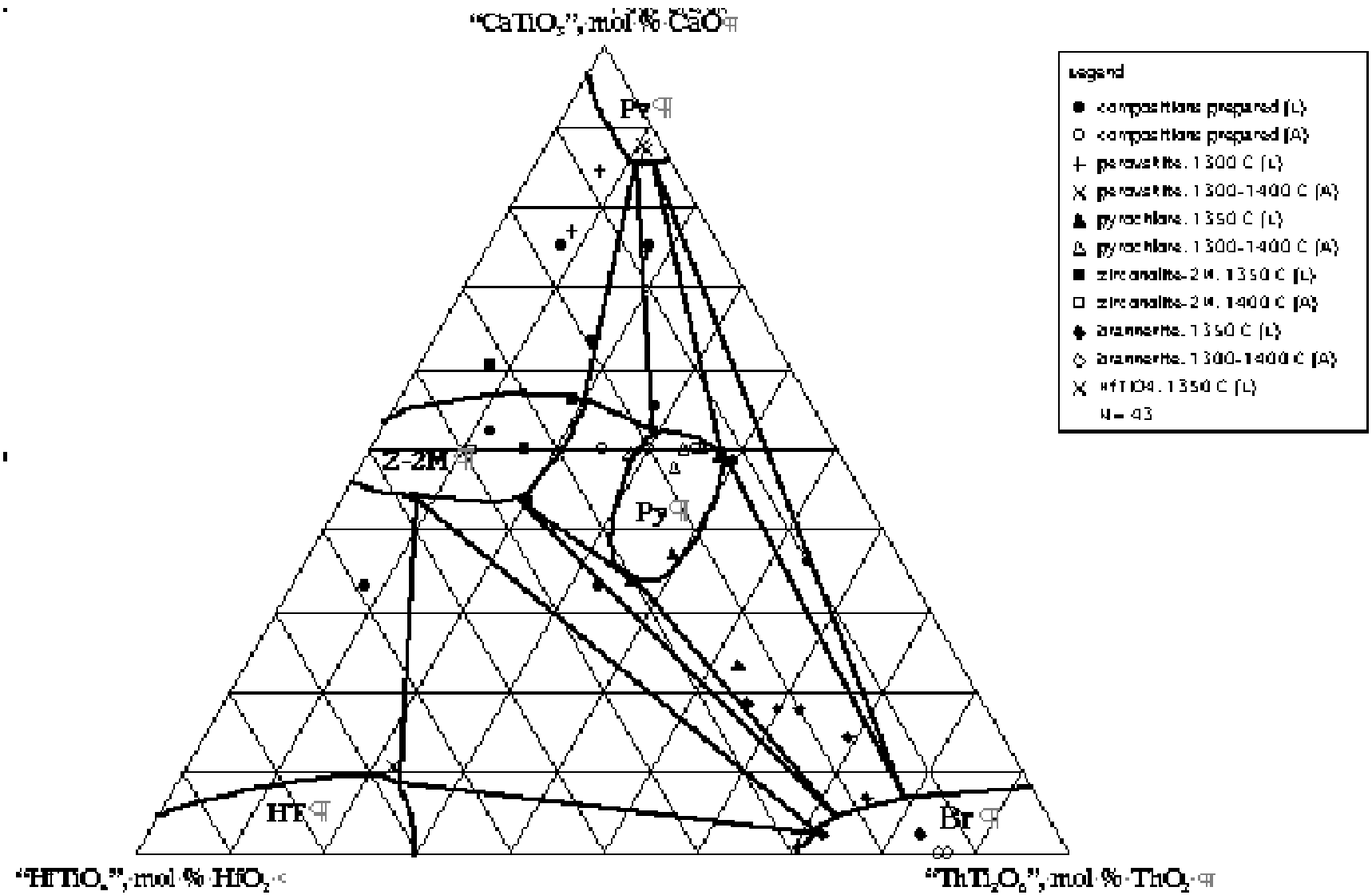

Figure 12. $GdTi_2O_7$-$CaThTi_2O_7$-$CaHfTi_2O_7$ phase diagram at 1350°C in air.

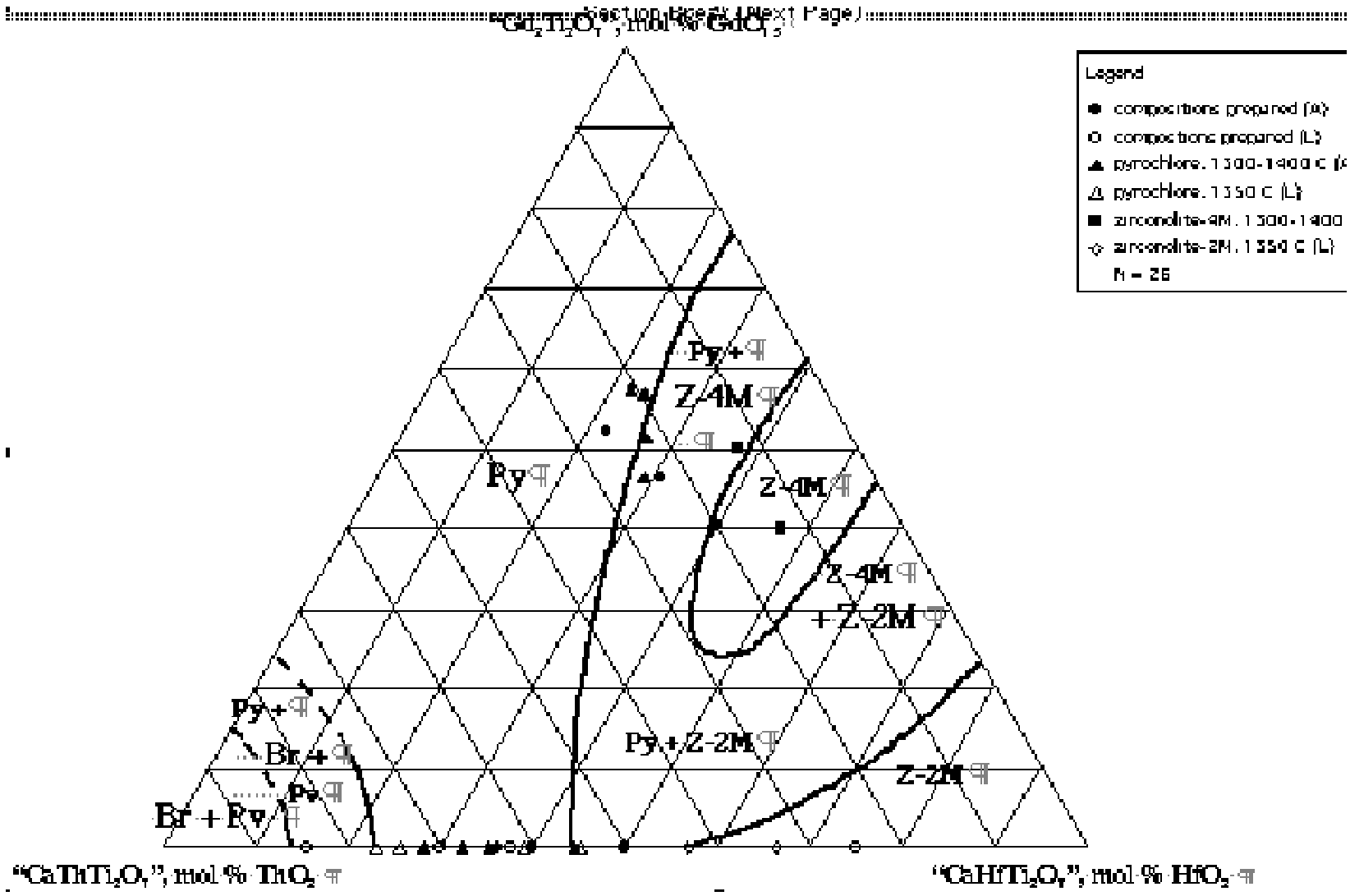

$CaTiO_3$-$HfTiO_4$-$AnTi_2O_6$ Phase Diagram at 1350°C in Air, An = U + Th + Gd

Samples for the $CaTiO_3$-$HfTiO_4$-$AnTi_2O_6$ phase diagram at 1350°C in air were prepared at LLNL (Ryerson 8/1 – Ryerson 8/3 in **Appendix A**) and at ANSTO (mws980268 – mws980288). The intent of the phase diagram (see **Figure 13**) is to show the phase relationships in a baseline formulation where Th is taken as a surrogate for plutonium. For plotting purposes Gd is included with U and Th as an actinide, i.e., An = U + Th + Gd. The pyrochlore and brannerite phases show reasonable agreement between the LLNL and ANSTO data. LLNL in one sample found a zirconolite-2M phase but did not find a zirconolite-4M phase in any of their 3 samples, while ANSTO in one sample found a zirconolite-4M phase but no zirconolite-2M in their 2 samples. Considering the limited amount of data, it is assumed that both zirconolite-2M and zirconolite-4M are present in the phase diagram. The perovskite and $HfTiO_4$ phases are put in as estimates. The hafnia content of rutile is 8 mol % in this phase diagram.

$CaTiO_3$-$HfTiO_4$-$AnTi_2O_6$ Phase Diagram at 1350°C and low O_2 pressures, An = U + Th + Gd

The $CaTiO_3$-$HfTiO_4$-$AnTi_2O_6$ phase diagram at 1350°C with $f_{O2} = 10^{-5.90}$ to $10^{-10.06}$ atm is given in **Figure 14**. This phase diagram shows the behavior of a baseline formulation where Th is taken as a surrogate for plutonium and reducing conditions prevail. Samples from LLNL are Ryerson 8/6 to Ryerson 8/9 in **Appendix A**. The phase diagram is generally similar to that in air (**Figure 13**), except there is no evidence for a zirconolite-4M phase, and the CaO solubility in brannerite is reduced. The solubilities of HfO_2 and AnO_2 in perovskite are assumed to be low. The rutile contains 6 mol % hafnia in these samples. There are also data from LLNL [13] on samples with $f_{O2} = 10^{-2.60}$ and $10^{-5.05}$ atm (not listed in **Appendix A**). The main difference from the data presented here is a higher CaO content in the brannerite phase.

Figure 13. $CaTiO_3$-$HfTiO_4$-$AnTi_2O_6$ phase diagram at 1350°C in air. An = U + Th + Gd.

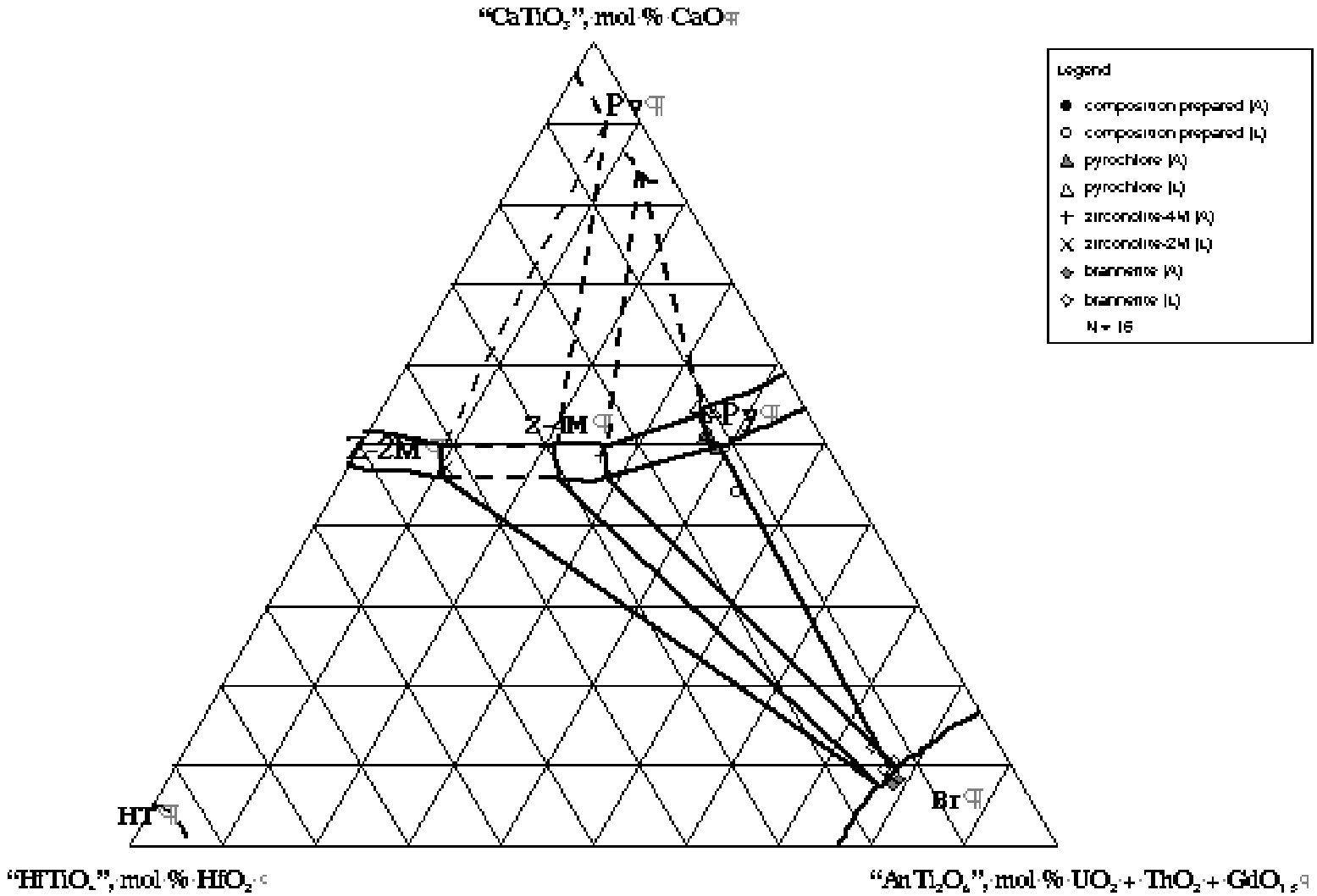

Figure 14. $CaTiO_3$-$HfTiO_4$-$AnTi_2O_6$ phase diagram at 1350°C and $f_{O2} = 10^{-5.90}$ to $10^{-10.06}$ atm. An = U+Th+Gd.

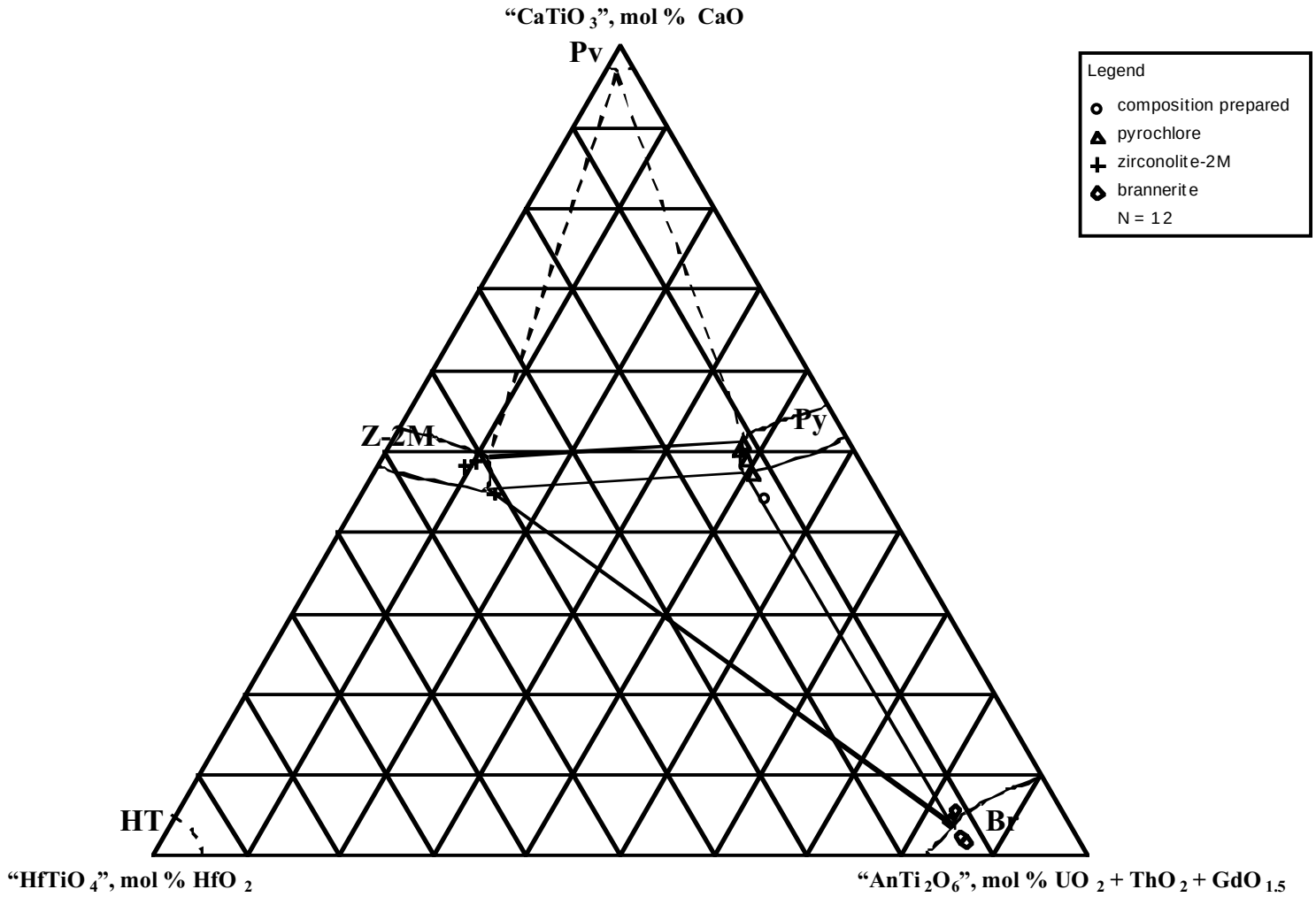

TiO_2-CaO-PuO_2 Phase Diagram at 1300°C in Air

The TiO_2-CaO-PuO_2 phase diagram at 1300°C in air is given in **Figure 15**. Data are listed as R00m026 (90% $CaPuTi_2O_7$ + 10% $CaTiO_3$) and R00m026 (90% $CaPuTi_2O_7$ + 10% TiO_2) in **Appendix A**. ANSTO reports [12] that the Pu brannerite, $PuTi_2O_6$, does not form by sintering in air at or below 1400°C, so it is not shown on this phase diagram. Pyrochlore and perovskite were found to form at near stoichiometric compositions and rutile showed a low solubility for calcia and plutonia.

TiO_2-CaO-PuO_2 Phase Diagram at 1500°C in Air

For the TiO_2-CaO-PuO_2 phase diagram at 1500°C in air see **Figure 16**. Data are from ANSTO and are listed as Pu08202 to Pu12901 in **Appendix A**. Brannerite is found to be stable at this temperature, pyrochlore and rutile appear the same as at 1300°C (see **Figure 15**), while perovskite shows a slightly increased solid solution range.

$CaTiO_3$-$HfTiO_4$-PuO_2 Phase Diagram at 1400°C in Air or Ar

The $CaTiO_3$-$HfTiO_4$-PuO_2 phase diagram at 1400°C in air or Ar is presented in **Figure 17**. Data in Ar are given by ANSTO as Pu1501A to Pu11701A in **Appendix A**, and data in air are given by LLNL as ME3730 and ME3732 in **Appendix A**. There should be no significant difference between the phase diagrams in air or Ar, since Pu should be in the +4 valence state in either case. Brannerite was not found to form at 1400°C, as was indicated above. Zirconolite-4M did form, and the pyrochlore and zirconolite-2M phases showed extended solid solution ranges. Perovskite showed about a 7 mol % solubility of PuO_2. This phase diagram is considerably different from those for the U systems shown in **Figures 3** and **4**. The hafnia content of rutile averaged about 8 mol %.

$Gd_2Ti_2O_7$-$CaPuTi_2O_7$-$CaHfTi_2O_7$ Phase Diagram at 1400°C in Air or Ar

Figure 18 gives the $Gd_2Ti_2O_7$-$CaPuTi_2O_7$-$CaHfTi_2O_7$ phase diagram at 1400°C in air or Ar. Data on samples Pu11501A to Pu11701A (heated in Ar) and sample ME3730 (heated in air) were given earlier in **Appendix A**, and samples Pu11201A to Pu11401A, Pu12301A (heated in Ar), and Pu12302A (heated in air) are added to **Appendix A**. Boundaries for the pyrochlore, zirconolite-4M and zirconolite-2M phases proceed uniformly with gadolinia additions to the $Gd_2Ti_2O_7$-$CaHfTi_2O_7$ binary, where the intercept values are taken from the U system (**Figure 5**). Rutile in this system has an average hafnia content of about 8 mol %.

Figure 15. TiO_2-CaO-PuO_2 phase diagram at 1300ºC in air.

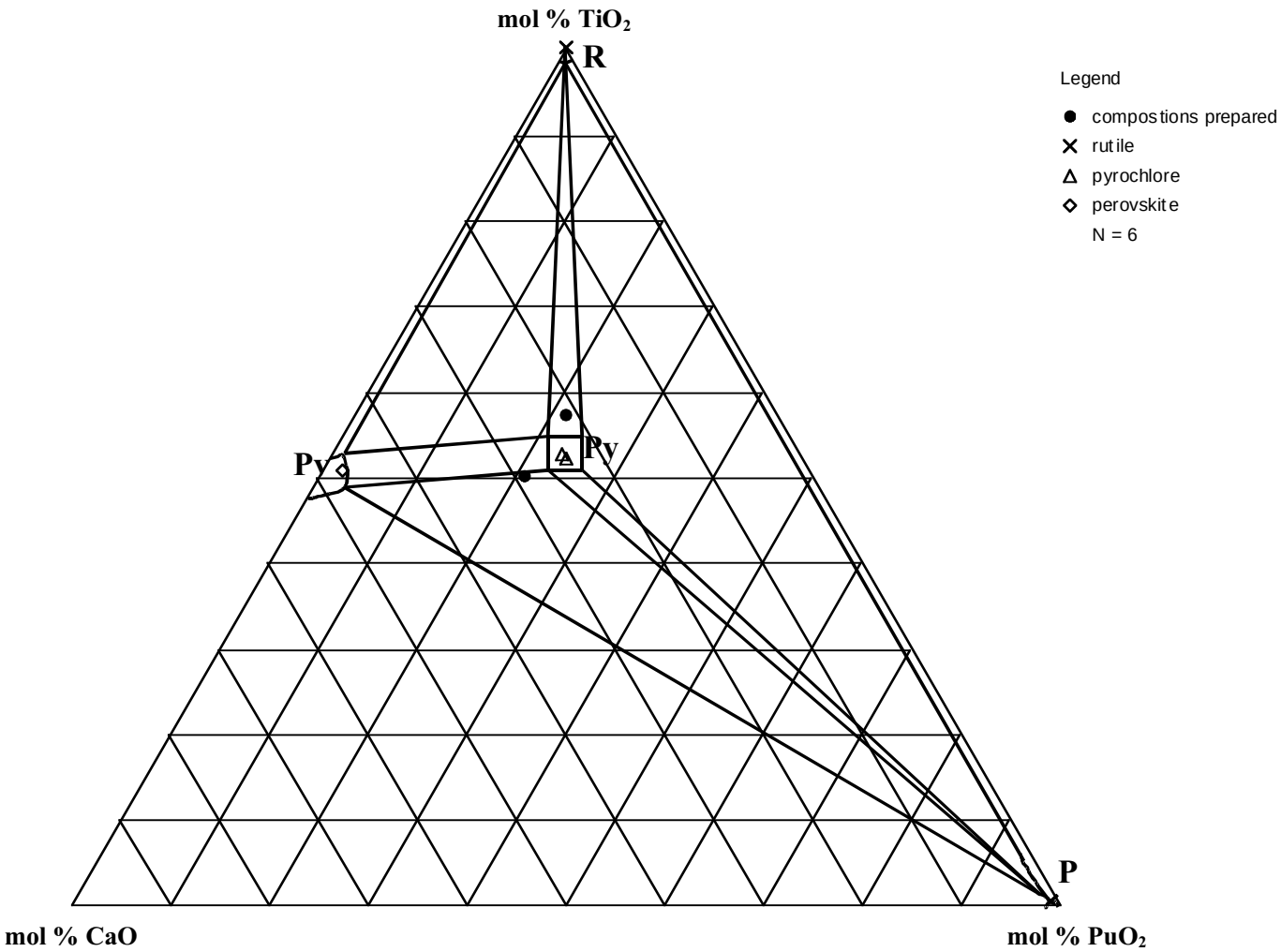

Figure 16. The TiO_2-CaO-PuO_2 phase diagram at 1500°C in air.

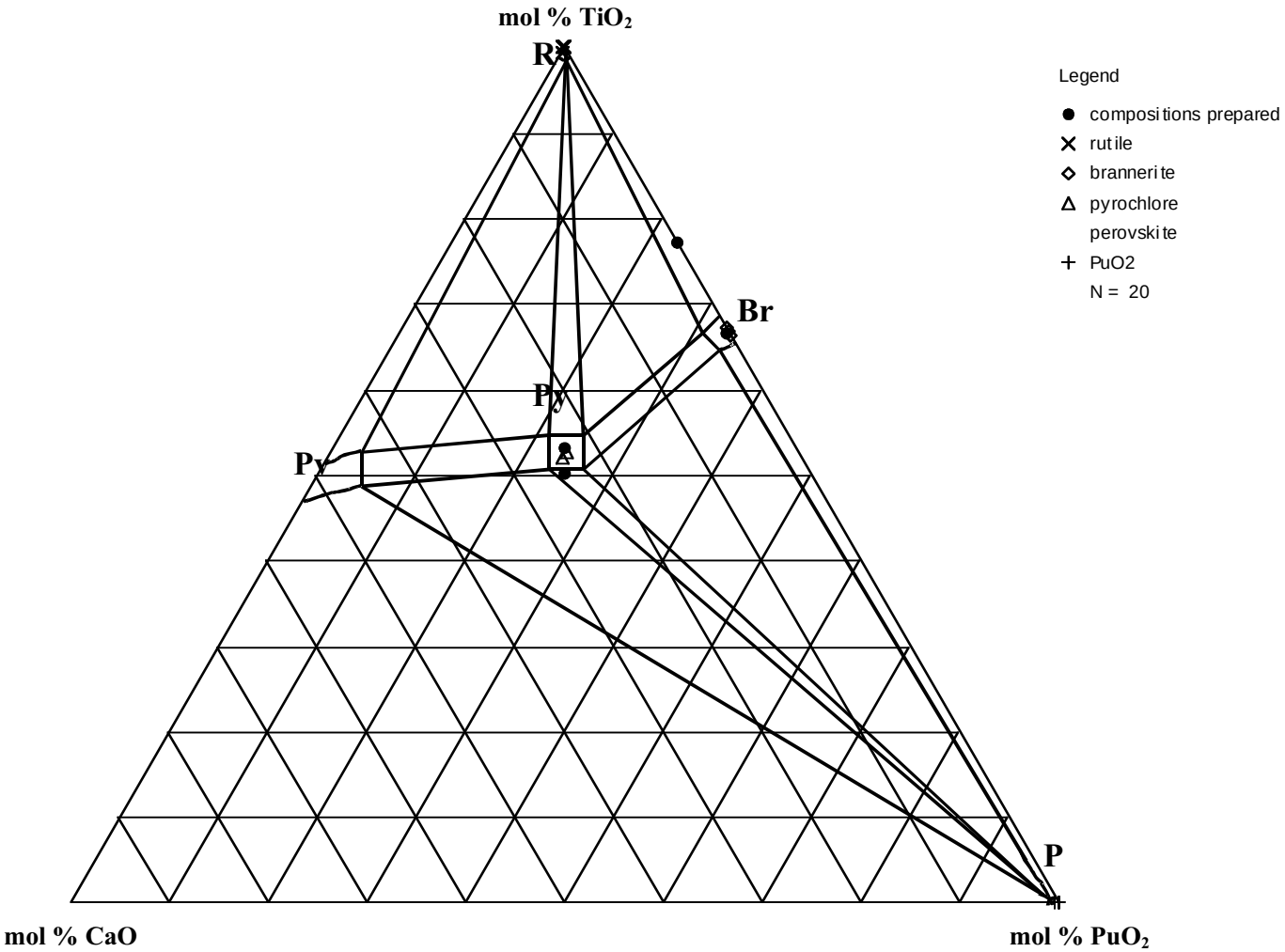

Figure 17. $CaTiO_3$-$HfTiO_4$-PuO_2 phase diagram at 1400°C in air or argon.

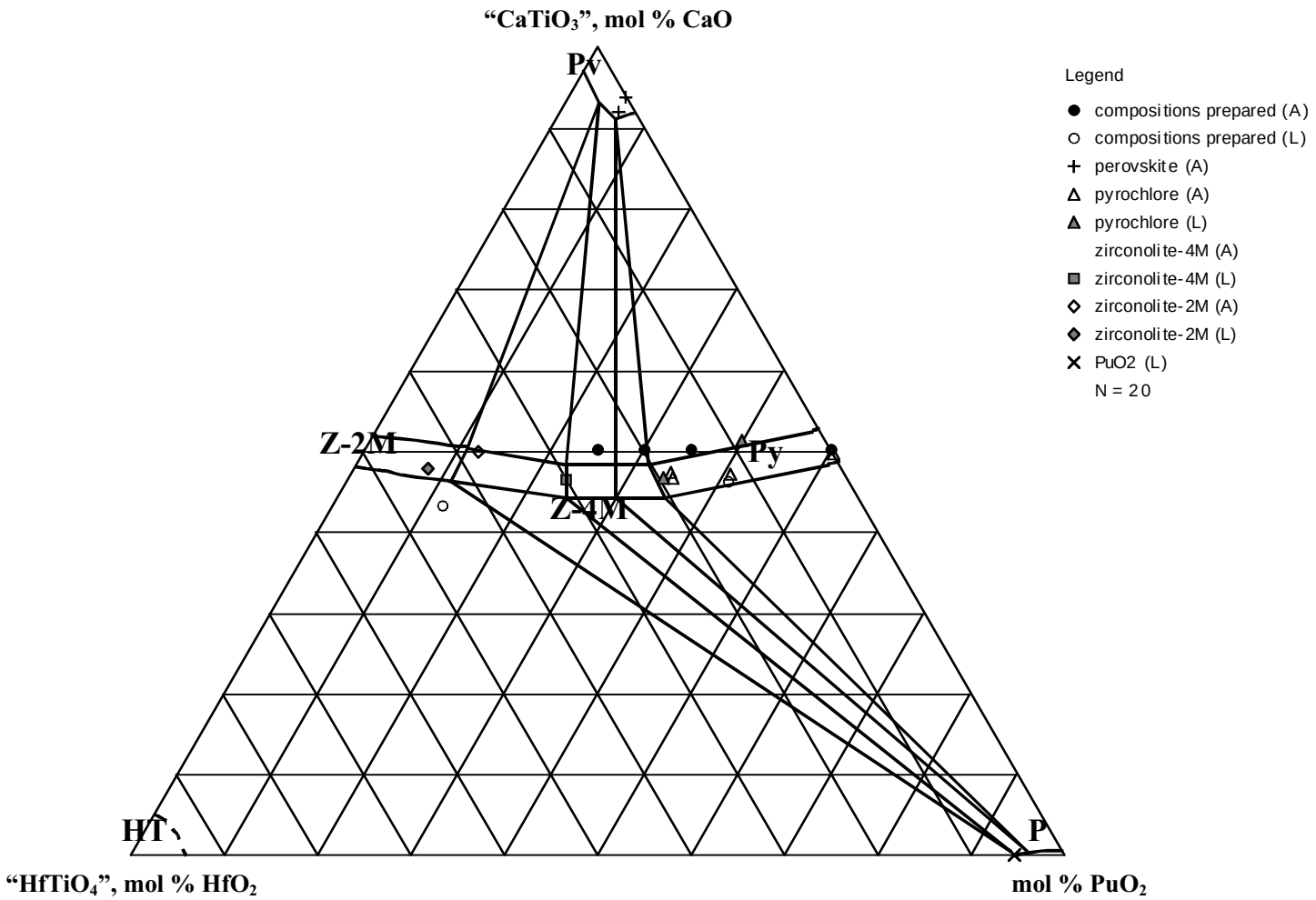

Figure 18. $Gd_2Ti_2O_7$-$CaPuTi_2O_7$-$CaHfTi_2O_7$ phase diagram at 1400°C in air or argon.

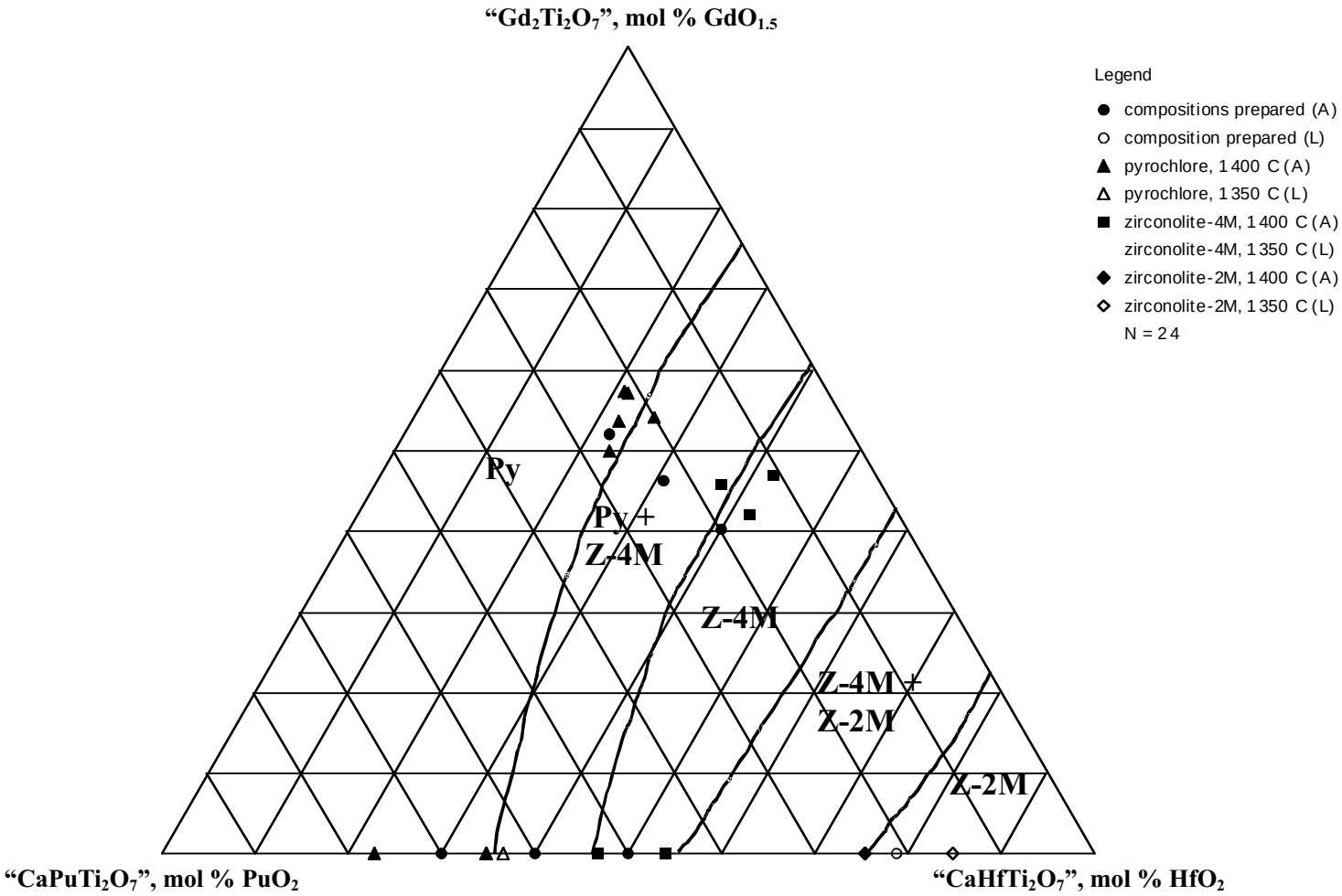

$CaTiO_3$-$HfTiO_4$-$AnTi_2O_6$ Phase Diagram at 1350°C in Air, An = U + Pu + Gd

This phase diagram (**Figure 19**) shows the relationship of phases in equilibrium with pyrochlore in the baseline formulation. It is similar to the phase diagram in **Figure 9**, where Ce was used as a surrogate for Pu. The main difference is a lower solubility of Pu in perovskite compared to Ce. LLNL samples used are ME3679Q to ME3688A in **Appendix A**, and ANSTO samples are R97m030 (1325C Wet Mill-Air) through R97m030 (1400C Dry Mill-Air) in **Appendix A**. The ANSTO samples show a lower content of CaO in the pyrochlore phase than do the LLNL samples. Al_2O_3 impurity in the samples may have been introduced from the starting materials, but some Al_2O_3 may also have been introduced during processing of the ANSTO samples. Enrichment of Al_2O_3 in zirconolite-2M is apparent in sample R97m030 (1325 Dry Milled). Residual amounts of actinide oxide were found in the samples and are primarily a mixed plutonium-uranium oxide with small amounts of calcia, gadolinia and hafnia usually present. Rutile has a hafnia content of about 10 mol % in this system.

$CaTiO_3$-$HfTiO_4$-$AnTi_2O_6$ Phase Diagram at 1350°C in Ar, An = U + Pu + Gd

The $CaTiO_3$-$HfTiO_4$-$AnTi_2O_6$ phase diagram at 1350°C in Ar (see **Figure 20**) shows very little difference from that in air (see **Figure 19**). Data are given in **Appendix A** on one LLNL sample, ME3688R, and ANSTO samples from R97m030 (1325°C Wet Mill-Ar) to the end of **Appendix A**. Zirconolite-2M formed in samples that had an intentional addition of Al_2O_3, and showed a lower actinide solubility than was the case in the air system. Brannerite had a lower CaO content than in the air system. Rutile has a hafnia content of 9.0 mol % and a urania content of 0.8 mol % averaged over a large number of samples. The plutonia content of the rutile was very low, usually below detectibility.

Figure 19. $CaTiO_3$-$HfTiO_4$-$AnTi_2O_6$ phase diagram at 1350°C in air. An = U + Pu + Gd.

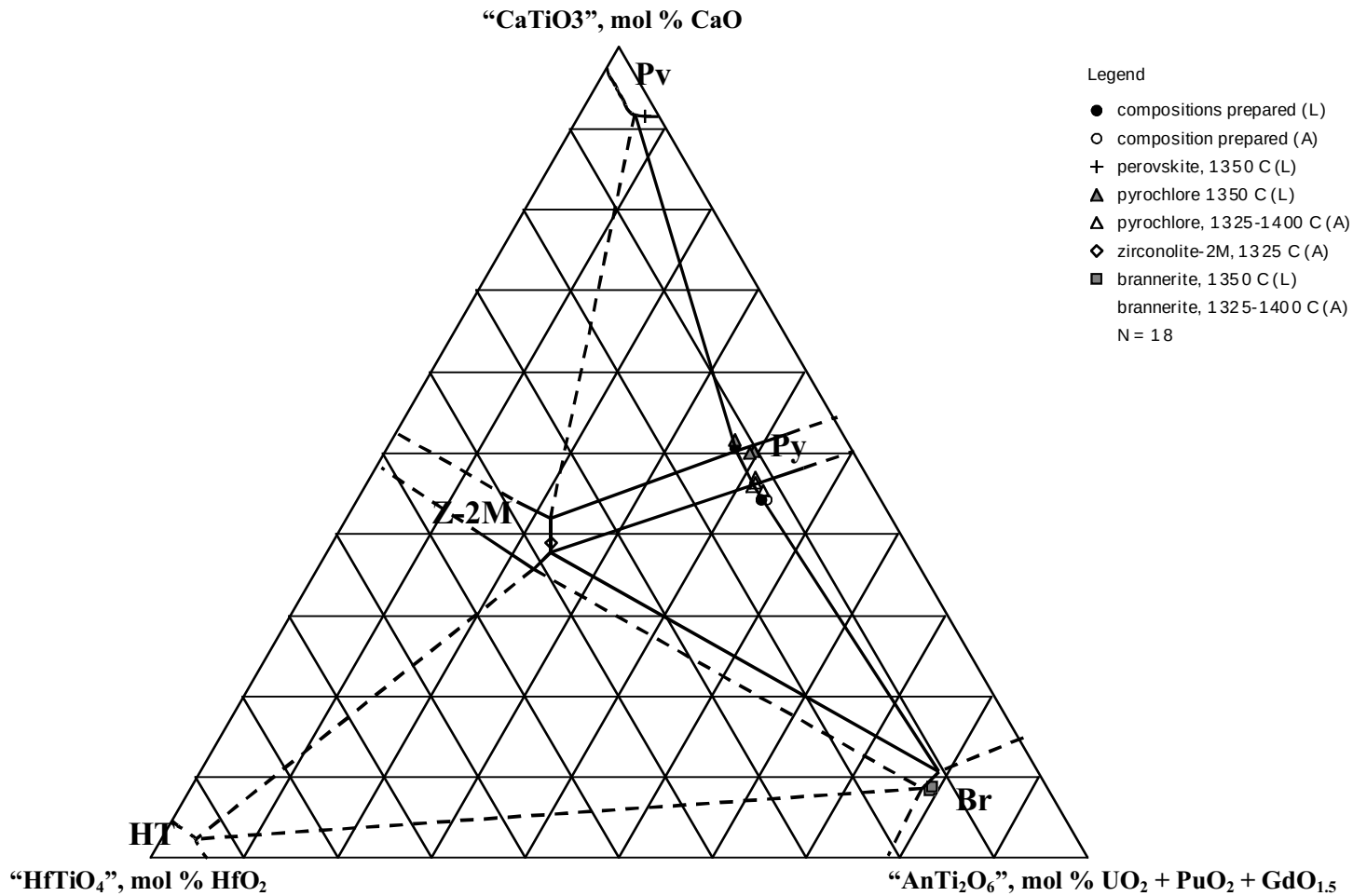

Figure 20. $CaTiO_3$-$HfTiO_4$-$AnTi_2O_6$ phase diagram at 1350°C in Ar. An = U + Pu + Gd.

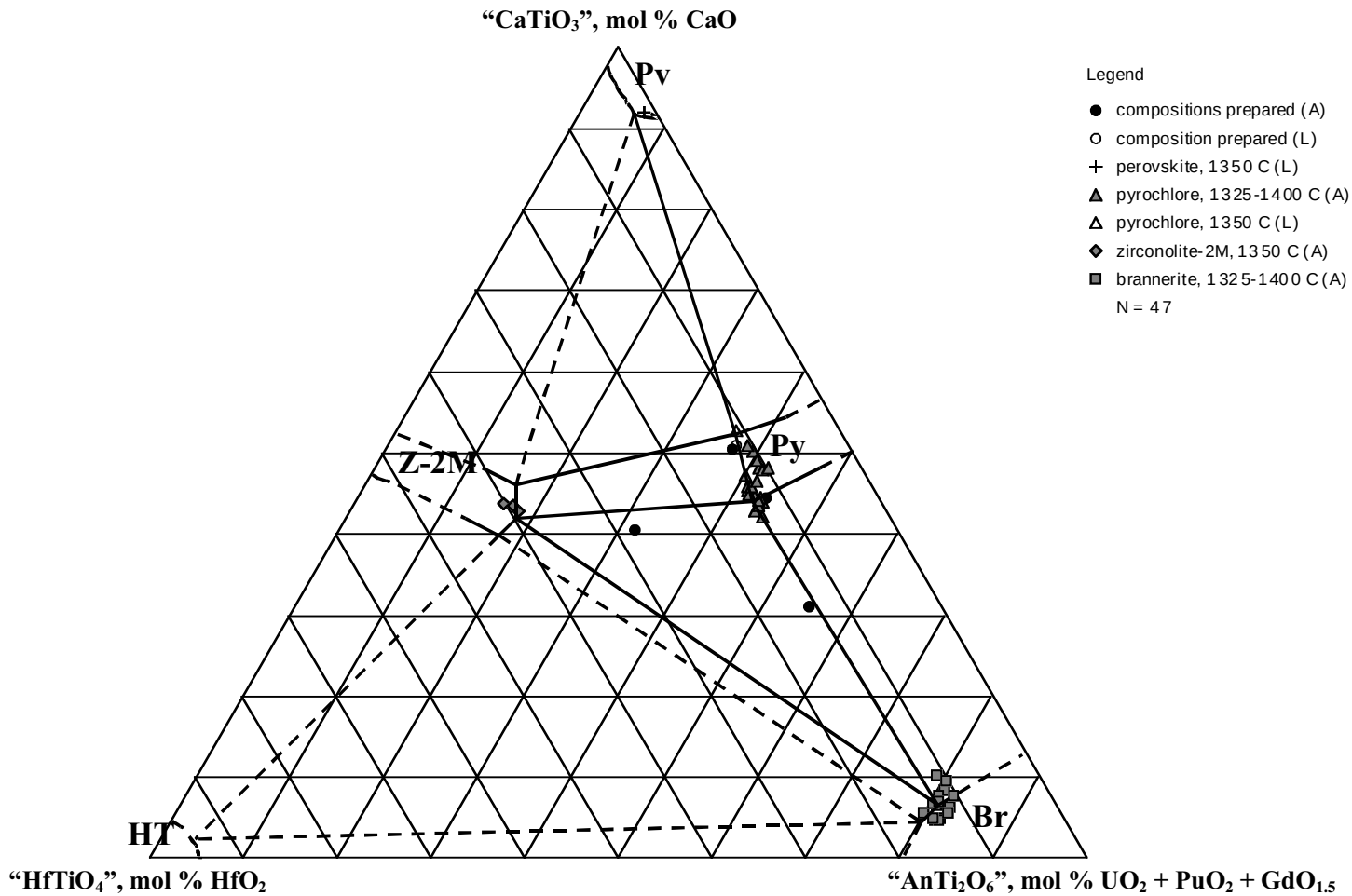

Summary and Conclusions

Overall, four types of phase diagrams have been determined. The first group of diagrams covers those in the group $CaO-TiO_2-AnO_2$ (An=Th, U, or Pu). These diagrams are shown in **Figures 3**, **4**, **10**, **15**, and **16**. With the exception of the stability and composition of the pyrochlore phase, the diagrams are nearly identical. In the Th system, **Figure 10**, pyrochlore does not form. In the U system, **Figures 3** and **4**, the pyrochlore is formed at an off-stoichiometric composition. In the Pu system, **Figures 15** and **16**, the pyrochlore occurs at very near stoichiometric composition.

The second type of phase diagrams are those in the group $Gd_2Ti_2O_7$-$CaHfTi_2O_7$-(Mg+Ti or Al_2)TiO_5. These diagrams are shown in **Figures 1** and **2**. Except for a slightly larger solid solubility of MgO in the zirconolite-3O phase than Al_2O_3 in the same phase, the two phase diagrams are essentially identical. This indicates that the effect of MgO and Al_2O_3 on the ceramic form are approximately the same. In combination with other work that shows that CoO, FeO, NiO, ZnO, and MgO partition roughly equally among the equilibrium phases and Gd_2O_3 and Al_2O_3 partition roughly evenly among the equilibrium phases, these data allow one to conclude that all of these impurities (at least in small quantities) have roughly the same effect on the ceramic system.

The third type of phase diagrams are those in the group $Gd_2Ti_2O_7$-(Ca,An)Ti_2O_7-$CaHfTi_2O_7$ (An = Th, U, or Pu). These diagrams are shown in **Figures 7**, **8**, **12**, and **18**. The diagrams are all similar. The Gd and actinide-rich portions of the diagrams are in all cases pyrochlore and the Hf-rich portions of the diagrams are zirconolite-2M. Intermediate in all cases is the zirconolite-4M. However, the region of stability of zirconolite-4M does not always extend to the actinide-rich portion of the diagram. Zirconolite-4M is most stable in the Pu system, **Figure 18**, and least stable in the Th system, **Figure 12**. Stability of zirconolite-4M in the U system, **Figures 7** and **8**, is highly dependent upon the redox conditions, with oxidizing conditions favoring the formation of zirconolite-4M.

The fourth and last type of phase diagrams are those in the group $CaTiO_3$-$HfTiO_4$-$AnTi_2O_6$ (An = Th, U, Pu, U+Ce+Gd, U+Th+Gd, or U+Pu+Gd). There are some differences in the end-member systems, e.g An = Th, U, or Pu, but the three intermediate systems, e.g. An = U+Ce+Gd, and U+Th+Pu, or U+Pu+Gd are very similar. In the end-member systems, there is some variation in the zirconolite-2M and pyrochlore phase boundaries. In the U-based system, **Figures 5** and **6**, the zirconolite-2M and pyrochlore phases are enriched in CaO, particularly when heat treated in air rather than argon atmosphere. The Th, **Figure 11**, and Pu, **Figure 17**, systems contain significantly less CaO in the zirconolite-2M and pyrochlore phases. Zirconolite-4M is only observed in the Pu-based system. And pyrochlore has a limited region of stability in the Th based system, **Figure 11**. In the intermediate systems, the U+Th+Gd system in air, **Figure 13**, can form zirconolite-4M, whereas under reducing conditions, **Figure 14**, zirconolite-4M is not stable

at any composition. Zirconolite-4M is not stable in either of the U+Ce+Gd, **Figure 9**, or the U+Pu+Gd systems, **Figures 19** and **20**. Besides a slight difference in the location of the zirconolite-2M and pyrochlore phase boundaries, these two systems are nearly identical.

These data along with the data for the Ce-based systems presented in another report [4], allow one to project the equilibrium phases for a numerous range of compositions that are at or near the composition selected for the plutonium immobilization ceramic. Projection of the equilibrium phases is one of the elements of the "Process Control Model" which will be used to "ensure that the ceramic immobilization process will produce an acceptable product."

References

1. B. B. Ebbinghaus, G. A. Armantrout, L. Gray, C. C. Herman, H. Shaw, and R. A. Van Konynenburg, "Plutonium Immobilization Project Baseline Formulation," Lawrence Livermore National Laboratory Report, UCRL-ID-133089, rev. 1, PIP-00-141, September 2000.

2. R. A. Van Konynenburg, et al., "Development of a Ceramic Form for the Immobilization of Excess Plutonium-Non Plutonium and Surrogate Studies," LLNL report to be published.

3. B. B. Ebbinghaus, et al, ""Development of a Ceramic Form for the Immobilization of Excess Plutonium-Plutonium Studies," LLNL report to be published.

4. S. I. Martin, O. H. Krikorian, B. B. Ebbinghaus, R. Putnam, E. R. Vance, and M. W. Stewart, "Synthesis and Characterization of Cerium Titanate and related Titanate Minerals in the Development of a Ceramic Waste Form," LLNL report to be published.

5. E. R. Vance, M. L. Carter and R. A. Day, "Interim Report on Task 1.1: Single-Phase Sample Production," Australian Nuclear Science and Technology Organisation Report, Report Number R99m022, April 20, 1999.

6. D. S. Perera, R. A. Day, M. W. A. Stewart and E. R. Vance, "Interim Report on Task 1.3: Equilibrium Phase Diagram," Australian Nuclear Science and Technology Organisation Report, Report Number R99065m, November 26, 1999.

7. D. S. Perera, R. A. Day, M. W. A. Stewart and E. R. Vance, "Interim Report on Task 1.3: Equilibrium Phase Diagram," Australian Nuclear Science and Technology Organisation Report, Report Number R00m015, March 31, 2000.

8. M. W. A. Stewart, E. R. Vance, A. Jostsons, P. A. Walls, K. P. Hart, S. Moricca, R. A. Day, G. R. Lumpkin. C. J. Ball, and D. S. Perera, "Final Report to Lawrence Livermore National Laboratory for Contract B345772," Australian Nuclear Science and Technology Organisation Report, Report Number R00m031, October 12, 2000.

9. R. S. Roth, T. Negas, and L. P. Cook, Phase Diagrams for Ceramists, Vol. IV, Fig. 5024, editor G. Smith, compiled at the National Bureau of Standards, Gaithersburg, Maryland, The American Ceramic Society, Columbus, Ohio, 1981.

10. Phase Diagrams for Ceramists, Vol. XII Oxides, Fig. 9897, editors A. E. McHale and R. S. Roth, compiled at the National Institute of Standards and Technology, Gaithersburg, Maryland, The American Ceramic Society, Westerville, Ohio, 1996.

11. E. R. Vance, M. W. A. Stewart, R. A. Day, K. P. Hart, M. J. Hambley and A. Brownscombe, "Pyrochlore-rich Titanate Ceramics for Incorporation of Plutonium, Uranium and Process Chemicals. Final Report," Australian Nuclear Science and Technology Organisation Report, Report Number R97m030, November 18, 1997.

12. B. D. Begg, M. Mestre, R. A. Day and E. R. Vance, "Task 1.3: Equilibrium Phase Diagram. Phase 3 (ii): Phase equilibria in the TiO_2-rich portion of the CaO-AnO_2-TiO_2 ternary (An = Ce, Th, U or Pu)," Australian Nuclear Science and Technology Organisation Report, Report Number R00m026, April 30, 2000.

13. F. J. Ryerson and B. B. Ebbinghaus, “Pyrochlore-rich Titanate Ceramics for the Immobilization of Plutonium: Redox Effects on Phase Equilibria in Cerium- and Thorium-substituted Analogs,” Lawrence Livermore National Laboratory Report, UCRL-ID-139092, May, 2000.

14. M. W. A. Stewart, E. R. Vance and R. A. Day, “Supplement to Interim Report on Task 1.3: Equilibrium Phase Diagram,” Australian Nuclear Science and Technology Organisation Report, Report Number R99m023, April 18, 1999.

15. M. W. A. Stewart, E. R. Vance and R. A. Day, “Report on Phase 2 of Task 1.1: Single Phase Synthesis,” Australian Nuclear Science and Technology Organisation Report, Report Number R99m063, November 23, 1999.

16. D. S. Perera, R. A. Day, M. W. A. Stewart and E. R. Vance, “Interim Report on Task 1.3: Equilibrium Phase Diagram,” Australian Nuclear Science and Technology Organisation Report, Report Number R99m021, April 19, 1999.

17. F. J. Ryerson, Lawrence Livermore National Laboratory, private communication for data on Ryerson samples 8/1 and 8/2, July, 2000.

18. M. W. A. Stewart, E. R. Vance, R. A. Day and A. Brownscombe, “Interim Report on Task 1.2: Near Equilibrium Processing Requirements, Parts 1 and 2,” Australian Nuclear Science and Technology Organisation Report, Report Number R99m012, April 5, 1999.

19. D. S. Perera, M. W. A. Stewart, R. A. Day, A. Brownscombe and E. R. Vance, “Update of Interim Report on Task 1.3: Equilibrium Phase Diagram,” Australian Nuclear Science and Technology Organisation Report, Report Number R99m037, July 30, 1999.

Appendix A

Electron Microprobe and Quantitative SEM-EDS Analyses

The relative atomic contents of metallic constituents are listed for each phase in **Tables A1** to **A151**. The oxygen content is calculated based upon assumed valences of the metallic constituents, i.e., Na and K are +1, Mg and Ca are +2, B, Al and Gd are +3, Si, Ti, Hf and Th are +4, and U is +5 for heatings in air and +4 for heatings in Ar or reduced oxygen pressures. Ce is taken as +4 in heatings in air except as +3 in perovskite, and is taken as +3 in heatings in Ar or reduced oxygen pressures. In the microprobe analyses, the total number of metal atoms is normalized to give the ideal total number of metal atoms in each structure. In the SEM/EDS analyses (taken from ANSTO) the number of metal atoms is normallized to give the ideal total number of oxygen atoms in each structure. The uncertainty in the microprobe analysis for the major constituents is estimated to be ± 0.004 atomic units and for the SEM/EDS analysis, ± 0.01 atomic units.

Table A1. Microprobe analysis of SM0623a [4].
Composition $Ca_{0.50}Hf_{0.50}GdTi_2O_{7.20}$ heated at 1350 ºC in air.

Phase	Ca	Hf	Gd	Ti	O	Total
Pyrochlore	0.4557	0.3785	1.1628	2.0030	6.9629	11.9629
Zirconolite-4M	0.5841	0.5579	0.8517	2.0063	6.9901	11.9901
HfO_2	0.0215	0.8611	0.0156	0.1018	1.9707	2.9707

Table A2. Microprobe analysis of SM0624a [4].
Composition $Ca_{0.35}Hf_{0.35}Gd_{1.30}Ti_{2.10}O_{7.20}$ heated at 1350 ºC in air.

Phase	Ca	Hf	Gd	Ti	O	Total
Pyrochlore	0.3623	0.3180	1.3063	2.0134	6.9846	10.9846
Rutile	0.0000	0.0675	0.0000	0.9325	2.0000	3.0000

Table A3. Microprobe analysis of SM1116a [4].
Composition $Ca_{0.20}Hf_{0.20}Gd_{1.60}Ti_{2.10}O_{7.20}$ heated at 1350 ºC in air.

Phase	Ca	Hf	Gd	Ti	O	Total
Pyrochlore	0.1885	0.1605	1.5960	2.0550	7.0135	11.0135
$HfTiO_4$	0.0065	0.9617	0.0370	0.9948	3.9750	5.9750
HfO_2	0.0121	0.7967	0.0422	0.1490	1.9668	2.9668

Table A4. Microprobe analysis of SM1116b [4].

Composition $Ca_{0.80}Hf_{0.80}Gd_{0.40}Ti_{2.10}O_{7.20}$ heated at 1350ºC in air.

Phase	Ca	Hf	Gd	Ti	O	Total
Zirconolite-4M	0.7594	0.6569	0.4847	2.0990	6.9983	10.9983
Zirconolite-2M	0.8497	0.9669	0.2462	1.9372	7.0272	11.0272
HfO_2	0.0454	0.7911	0.0195	0.1440	1.9449	2.9449

Table A5. Quantitative SEM/EDS analysis of mws980401 [14].

Composition $Ca_{0.50}Hf_{0.50}GdTi_{3.12}O_{9.24}$ heated at 1500ºC in air.

Phase	Ca	Hf	Gd	Ti	O	Total
Pyrochlore	0.46	0.35	1.14	2.06	7.00	11.01
zirconolite-4M	0.58	0.49	0.79	2.13	7.00	10.99
Rutile		0.08		0.92	2.00	3.00

Table A6. Quantitative SEM/EDS analysis of mws980402 [14].

Composition $Ca_{0.45}Hf_{0.45}Gd_{1.10}Ti_2O_7$ heated at 1500ºC in air.

Phase	Ca	Hf	Gd	Ti	O	Total
Pyrochlore	0.44	0.40	1.19	1.98	7.00	11.01
zirconolite-4M	0.54	0.57	0.86	1.98	7.00	10.95
Rutile		0.11		0.89	2.00	3.00

Table A7. Quantitative SEM/EDS analysis of mws980422 [14].

Composition $Ca_{0.50}Hf_{0.545}GdTi_2O_{7.09}$ heated at 1500ºC in air.

Phase	Ca	Hf	Gd	Ti	O	Total
Pyrochlore	0.42	0.42	1.19	1.97	7.00	11.00
zirconolite-4M	0.53	0.59	0.86	2.00	7.00	10.98
Rutile		0.11		0.89	2.00	3.00

Table A8. Quantitative SEM/EDS analysis of mws980423 [14].

Composition $Ca_{0.60}Hf_{0.60}Gd_{0.80}Ti_2O_7$ heated at 1500ºC in air.

Phase	Ca	Hf	Gd	Ti	O	Total
zirconolite-4M	0.57	0.56	0.80	2.05	7.00	10.98
Rutile		0.11		0.89	2.00	3.00

Table A9. Quantitative SEM/EDS analysis of mws980424 [14].

Composition $Ca_{0.70}Hf_{0.70}Gd_{0.60}Ti_2O_7$ heated at 1500ºC in air.

Phase	Ca	Hf	Gd	Ti	O	Total
zirconolite-4M	0.68	0.66	0.63	2.02	7.00	10.99
Rutile		0.13		0.89	2.00	3.02

Table A10. Quantitative SEM/EDS analysis of mws980425 [14].

Composition $Ca_{0.80}Hf_{0.80}Gd_{0.40}Ti_2O_7$ heated at 1500°C in air.

Phase	Ca	Hf	Gd	Ti	O	Total
zirconolite-4M	0.72	0.66	0.56	2.05	7.00	10.99
zirconolite-2M	0.80	0.83	0.29	2.05	7.00	10.97
Rutile		0.14		0.86	2.00	3.00

Table A11. Quantitative SEM/EDS analysis of L990657 [6].

Composition $Gd_{1.80}Al_{0.20}Ti_{1.90}O_{6.80}$ heated at 1400°C in air.

Phase	Gd	Al	Ti	O	Total
Pyrochlore	1.909	0.096	1.997	7.000	11.001
Al_2TiO_5	0.084	1.936	0.985	5.000	8.005

Table A12. Quantitative SEM/EDS analysis of L990658 [6].

Composition $Ca_{0.20}Hf_{0.20}Gd_{1.40}Al_{0.20}Ti_{1.90}O_{6.80}$ heated at 1400 °C in air.

Phase	Ca	Hf	Gd	Al	Ti	O	Total
Pyrochlore	0.199	0.113	1.618	0.089	2.008	7.000	11.026
zirconolite-3O	0.211	0.274	0.895	0.735	1.898	7.000	11.013

Table A13. Quantitative SEM/EDS analysis of L990659 [6].

Composition $Ca_{0.40}Hf_{0.40}GdAl_{0.20}Ti_{1.90}O_{6.80}$ heated at 1400°C in air.

Phase	Ca	Hf	Gd	Al	Ti	O	Total
Pyrochlore	0.355	0.249	1.303	0.085	2.033	7.000	11.025
zirconolite-3O	0.447	0.496	0.638	0.523	1.911	7.000	11.014

Table A14. Quantitative SEM/EDS analysis of L990660 [6].

Composition $Ca_{0.60}Hf_{0.60}Gd_{0.60}Al_{0.20}Ti_{1.90}O_{6.80}$ heated at 1400°C in air.

Phase	Ca	Hf	Gd	Al	Ti	O	Total
zirconolite-3O	0.561	0.575	0.614	0.299	1.958	7.000	11.009
Perovskite	0.600	0.018	0.264	0.062	0.937	3.000	4.882

Table A15. Quantitiative SEM/EDS analysis of L990661 [6].

Composition $Ca_{0.80}Hf_{0.80}Gd_{0.20}Al_{0.20}Ti_{1.90}O_{6.80}$ heated at 1400°C in air.

Phase	Ca	Hf	Gd	Al	Ti	O	Total
Zirconolite-2M	0.780	0.762	0.231	0.237	1.997	7.000	11.007
Rutile	0.010	0.066	0.002	0.008	0.921	2.000	3.008

Table A16. Quantitative SEM/EDS analysis of L990669 [6].

Composition $Gd_{1.8}Al_{0.2}Ti_{1.9}O_{6.8}$ heated at 1300ºC in air.

Phase	Gd	Al	Ti	O	Total
Pyrochlore	1.911	0.089	2.000	7.000	11.000
$GdAlTi_4O_{11}$	1.119	1.020	3.896	11.000	17.035

Table A17. Quantitative SEM/EDS analysis of L990671 [6].

Composition $Ca_{0.80}Hf_{0.80}Gd_{0.20}Al_{0.20}Ti_{1.90}O_{6.80}$ heated at 1300ºC in air.

Phase	Ca	Hf	Gd	Al	Ti	O	Total
zirconolite-2M	0.786	0.780	0.230	0.235	1.978	7.000	11.009
Rutile		0.052			9.948	2.000	3.000

Table A18. Quantitative SEM/EDS analysis of L990674 [6].

Composition $Ca_{0.20}Hf_{0.20}Gd_{1.40}Al_{0.20}Ti_{1.90}O_{6.80}$ heated at 1350ºC in air.

Phase	Ca	Hf	Gd	Al	Ti	O	Total
Pyrochlore	0.175	0.096	1.629	0.105	2.016	7.000	11.021
zirconolite-3O	0.228	0.309	0.828	0.787	1.867	7.000	11.017

Table A19. Quantitative SEM/EDS analysis of L990675 [6].

Composition $Ca_{0.60}Hf_{0.60}Gd_{0.60}Al_{0.20}Ti_{1.90}O_{6.80}$ heated at 1350ºC in air.

Phase	Ca	Hf	Gd	Al	Ti	O	Total
zirconolite-3O	0.564	0.534	0.671	0.271	1.977	7.000	11.018
Perovskite	0.608	0.019	0.259	0.066	0.934	3.000	4.885

Table A20. Quantitative SEM/EDS analysis of L990820 [7].

Composition $Ca_{0.10}Hf_{0.10}Gd_{1.40}Al_{0.40}Ti_{1.80}O_{6.60}$ heated at 1400ºC in air.

Phase	Ca	Hf	Gd	Al	Ti	O	Total
pyrochlore	0.137	0.109	1.700	0.098	1.974	7.000	11.018
zirconolite-3O	0.126	0.278	0.911	0.879	1.817	7.000	11.010
Al_2TiO_5	0.004	0.005	0.026	1.950	1.011	5.000	7.996

Table A21. Quantitative SEM/EDS analysis of L990821 [7].

Composition $Ca_{0.40}Hf_{0.40}Gd_{0.80}Al_{0.40}Ti_{1.80}O_{6.60}$ heated at 1400ºC in air.

Phase	Ca	Hf	Gd	Al	Ti	O	Total
pyrochlore	0.341	0.218	1.369	0.093	2.015	7.000	11.036
zirconolite-3O	0.384	0.486	0.673	0.610	1.859	7.000	11.013
Perovskite	0.570	0.010	0.318	0.119	0.877	3.000	4.894

Table A22. Quantitative SEM/EDS analysis of L990822 [7].

Composition $Ca_{0.60}Hf_{0.60}Gd_{0.40}Al_{0.40}Ti_{1.80}O_{6.60}$ heated at 1400ºC in air.

Phase	Ca	Hf	Gd	Al	Ti	O	Total
zirconolite-3O	0.550	0.548	0.453	0.471	1,984	7.000	11.006
zirconolite-2M	0.616	0.697	0.397	0.399	1.898	7.000	11.007
Perovskite	0.770	0.008	0.169	0.083	0.919	3.000	4.948

Table A23. Quantitative SEM/EDS analysis of L990823 [7].

Composition $Ca_{0.20}Hf_{0.20}GdAl_{0.40}Ti_{1.70}O_{6.10}$ heated at 1400ºC in air.

Phase	Ca	Hf	Gd	Al	Ti	O	Total
Pyrochlore	0.207	0.115	1.575	0.091	2.032	7.000	11.020
zirconolite-3O	0.232	0.293	0.800	0.781	1.905	7.000	11.011

Table A24. Quantitative SEM/EDS analysis of L990824 [7].

Composition $Ca_{0.50}Hf_{0.50}Gd_{0.40}Al_{0.60}Ti_{1.80}O_{6.60}$ heated at 1400ºC in air.

Phase	Ca	Hf	Gd	Al	Ti	O	Total
zirconolite-3O	0.556	0.538	0.467	0.498	1.961	7.000	11.019
Perovskite	0.742	0.007	0.183	0.098	0.912	3.000	4.941

Table A25. Microprobe analysis of mws990495 at LLNL.

Composition $Ca_{0.50}HfGd_{0.50}Al_{0.50}Ti_{1.59}O_{7.18}$ heated at 1350ºC in air [15].

Phase	Ca	Hf	Gd	Al	Ti	O	Total
zirconolite-2M	0.4850	0.9642	0.4896	0.4879	1.5733	7.0263	11.0263
$HfTiO_4$	0.0415	0.8910	0.0464	0.0496	0.9715	3.9105	5.9105

Table A26. Quantitative SEM/EDS analysis of L990662 [6].

Composition $Gd_{1.80}Mg_{0.10}Ti_2O_{6.80}$ heated at 1400ºC in air.

Phase	Gd	Mg	Ti	O	Total
Pyrochlore	1.789	0.192	2.062	7.000	11.043

Table A27. Quantitative SEM/EDS analysis of L990663 [6].

Composition $Ca_{0.20}Hf_{0.20}Gd_{1.40}Mg_{0.10}Ti_2O_{6.80}$ heated at 1400ºC in air.

Phase	Ca	Hf	Gd	Mg	Ti	O	Total
Pyrochlore	0.204	0.161	1.448	0.171	2.065	7.000	11.050
Rutile		0.030			0.970	2.000	3.000

Table A28. Quantitative SEM/EDS analysis of L990664 [6].

Composition $Ca_{0.40}Hf_{0.40}GdMg_{0.10}Ti_2O_{6.80}$ heated at 1400ºC in air.

Phase	Ca	Hf	Gd	Mg	Ti	O	Total
zirconolite-3O	0.401	0.391	0.975	0.081	2.137	7.000	10.985
Rutile		0.045			0.955	2.000	3.000

Table A29. Quantitative SEM/EDS analysis of L990665 [6].

Composition $Ca_{0.60}Hf_{0.60}Gd_{0.60}Mg_{0.10}Ti_2O_{6.80}$ heated at 1400ºC in air.

Phase	Ca	Hf	Gd	Mg	Ti	O	Total
zirconolite-3O	0.537	0.551	0.719	0.175	2.054	7.000	11.036
zirconolite-2M	0.545	0.721	0.525	0.214	2.006	7.000	11.011
Rutile		0.078			0.922	2.000	3.000

Table A30. Quantitative SEM/EDS analysis of L990666 [6].

Composition $Ca_{0.80}Hf_{0.80}Gd_{0.20}Mg_{0.10}Ti_2O_{6.80}$ heated at 1400ºC in air.

Phase	Ca	Hf	Gd	Mg	Ti	O	Total
zirconolite-2M	0.794	0.738	0.228	0.116	2.136	7.000	11.012
Rutile		0.065			0.935	2.000	3.000

Table A31. Quantitative SEM/EDS analysis of L990690 [6].

Composition $Gd_{1.80}Mg_{0.10}Ti_2O_{6.80}$ heated at 1300ºC in air.

Phase	Gd	Mg	Ti	O	Total
Pyrochlore	1.789	0.166	2.075	7.000	11.030

Table A32. Quantitiative SEM/EDS analysis of L990691 [6].

Composition $Ca_{0.40}Hf_{0.40}GdMg_{0.10}Ti_2O_{6.80}$ heated at 1300ºC in air.

Phase	Ca	Hf	Gd	Mg	Ti	O	Total
zirconolite-3O	0.395	0.372	0.968	0.242	2.083	7.000	11.061
Rutile		0.041			0.959	2.000	3.000

Table A33. Quantitative SEM/EDS analysis of L990692 [6].

Composition $Ca_{0.80}Hf_{0.80}Gd_{0.20}Mg_{0.10}Ti_2O_{6.80}$ heated at 1300ºC in air.

Phase	Ca	Hf	Gd	Mg	Ti	O	Total
zirconolite-2M	0.787	0.742	0.223	0.127	2.133	7.000	11.013
Rutile		0.057			0.943	2.000	3.000

Table A34. Quantitative SEM/EDS analysis of L990693 [6].

Composition $Ca_{0.20}Hf_{0.20}Gd_{1.40}Mg_{0.10}Ti_2O_{6.80}$ heated at 1350ºC in air.

Phase	Ca	Hf	Gd	Mg	Ti	O	Total
Pyrochlore	0.204	0.164	1.437	0.214	2.049	7.000	11.069
zirconolite-3O	0.200	0.411	0.861	0.486	2.101	7.000	11.058
Rutile		0.028			0.972	2.000	3.000

Table A35. Quantitative SEM/EDS analysis of L990694 [6].

Composition $Ca_{0.60}Hf_{0.60}Gd_{0.60}Mg_{0.10}Ti_2O_{6.80}$ heated at 1350ºC in air.

Phase	Ca	Hf	Gd	Mg	Ti	O	Total
zirconolite-3O	0.537	0.590	0.690	0.182	2.033	7.000	11.032
zirconolite-2M	0.548	0.772	0.511	0.231	1.955	7.000	11.017
Rutile		0.077			0.923	2.000	3.000

Table A36. Quantitative SEM/EDS analysis of L990815 [6].

Composition $Ca_{0.10}Hf_{0.10}Gd_{1.40}Mg_{0.20}Ti_2O_{6.60}$ heated at 1400ºC in air.

Phase	Ca	Hf	Gd	Mg	Ti	O	Total
pyrochlore	0.122	0.093	1.567	0.303	2.019	7.000	11.105
$MgTi_2O_5$	0.001	0.023	0.009	0.983	1.979	5.000	7.994

Table A37. Quantitative SEM/EDS analysis of L990816 [6].

Composition $Ca_{0.40}Hf_{0.40}Gd_{0.80}Mg_{0.20}Ti_2O_{6.60}$ heated at 1400ºC in air.

Phase	Ca	Hf	Gd	Mg	Ti	O	Total
zirconolite-3O	0.349	0.419	0.819	0.346	2.119	7.000	11.052
Perovskite	0.623	0.011	0.238	0.064	0.968	3.000	4.903

Table A38. Quantitative SEM/EDS analysis of L990817 [7].

Composition $Ca_{0.60}Hf_{0.60}Gd_{0.40}Mg_{0.20}Ti_2O_{6.60}$ heated at 1400ºC in air.

Phase	Ca	Hf	Gd	Mg	Ti	O	Total
zirconolite-2M	0.557	0.672	0.446	0.299	2.065	7.000	11.040
Perovskite	0.730	0.008	0.162	0.041	0.984	3.000	4.926

Table A39. Quantitative SEM/EDS analysis of L990818 [7].

Composition $Ca_{0.20}Hf_{0.20}GdMg_{0.30}Ti_2O_{6.40}$ heated at 1400ºC in air.

Phase	Ca	Hf	Gd	Mg	Ti	O	Total
Pyrochlore	0.227	0.134	1.365	0.229	2.114	7.000	11.069
zirconolite-3O	0.234	0.320	0.768	0.503	2.236	7.000	11.060
$MgTi_2O_5$	0.003	0.027	0.005	0.998	1.968	5.000	8.002

Table A40. Quantitative SEM/EDS analysis of L990819 [7].
Composition $Ca_{0.50}Hf_{0.50}Gd_{0.40}Mg_{0.30}Ti_2O_{6.40}$ heated at 1400ºC in air.

Phase	Ca	Hf	Gd	Mg	Ti	O	Total
zirconolite-2M'	0.497	0.532	0.494	0.346	2.176	7.000	11.045
zirconolite-2M	0.545	0.659	0.441	0.323	2.077	7.000	11.044
Perovskite	0.740	0.012	0.156	0.044	0.979	3.000	4.931
$MgTi_2O_5$	0.023	0.064	0.010	1.004	1.916	5.000	8.016

Table A41. Microprobe analysis of mws990491 at LLNL.
Composition $Ca_{0.40}HfGd_{0.60}Mg_{0.30}Ti_{1.76}O_{7.12}$ heated at 1350ºC in air [15].

Phase	Ca	Hf	Gd	Mg	Ti	O	Total
zirconolite-2M	0.4052	0.9721	0.5747	0.2914	1.7566	7.0161	11.0161
$HfTiO_4$	0.0213	1.0377	0.0396	0.0358	0.8657	3.9232	5.9232

Table A42. SEM/EDS analysis of R00m026 (90% UTi_2O_6 + 10% $CaTiO_3$) [12]. Composition $Ca_{0.28}U_{0.81}Ti_{1.91}O_{5.72}$ heated at 1400ºC in air.

Phase	Ca	U	Ti	O	Total
Brannerite	0.262	0.721	1.967	6.00	8.95

Table A43. Quantitative SEM/EDS analysis of R00m026 ($CaUTi_2O_7$) [12].
Composition $CaUTi_2O_7$ heated at 1350ºC in air.

Phase	Ca	U	Ti	O	Total
Pyrochlore	1.354	0.831	1.784	7.00	10.97
Brannerite	0.285	0.722	1.956	6.00	8.96

Table A44. Quantitative SEM/EDS analysis of R00m026 (90%$CaUTi_2O_7$+10%$CaTiO_3$) [12].
Composition $Ca_{1.17}U_{0.83}Ti_2O_{6.83}$ heated at 1350ºC in air.

Phase	Ca	U	Ti	O	Total
Pyrochlore	1.372	0.805	1.808	7.00	10.98
Brannerite	0.262	0.757	1.922	6.00	8.94
Rutile		0.020	0.975	2.00	3.00

Table A45. Microprobe analysis of P199A.
Composition $Ca_{0.246}U_{0.246}Ti_{0.508}O_{1.754}$ heated at 1400ºC in Ar.

Phase	Ca	U	Ti	O	Total
Pyrochlore	1.4539	0.7393	1.8068	6.5461	10.5461
Brannerite	0.1274	0.8654	2.0072	5.8726	8.8726
UO_2	0.3064	0.6768	0.0168	1.6936	2.6936

Table A46. Microprobe analysis of P201A.

Composition $Ca_{0.25}U_{0.20}Ti_{0.55}O_{1.75}$ heated at 1400°C in Ar.

Phase	Ca	U	Ti	O	Total
Pyrochlore	1.4639	0.6960	1.8401	6.5361	10.5361
Rutile	0.0000	0.0012	0.9988	2.0000	3.0000

Table A47. Microprobe analysis of P248.

Composition $Ca_{0.31}U_{0.20}Ti_{0.49}O_{1.69}$ heated at 1350°C in Ar.

Phase	Ca	U	Ti	O	Total
Pyrochlore	1.4708	0.7443	1.7849	6.5292	10.5292
Brannerite	0.1245	0.8660	2.0094	5.8753	8.8753
UO_2	0.3229	0.6574	0.0197	1.6771	2.6771

Table A48. Microprobe analysis of P249.

Composition $Ca_{0.29}U_{0.16}Ti_{0.55}O_{1.71}$ heated at 1350°C in Ar.

Phase	Ca	U	Ti	O	Total
Pyrochlore	1.4594	0.6917	1.8489	6.5406	10.5406
Rutile	0.0169	0.0101	0.9730	1.9831	2.9831

Table A49. Microprobe analysis of P250.

Composition $Ca_{0.24}U_{0.15}Ti_{0.61}O_{1.76}$ heated at 1350°C in Ar.

Phase	Ca	U	Ti	O	Total
Pyrochlore	1.4673	0.6905	1.8422	6.5327	10.5327
Brannerite	0.2791	0.6805	2.0404	5.7209	8.7209
Rutile	0.0000	0.0022	0.9978	2.0000	3.0000

Table A50. Microprobe analysis of P287.

Composition $Ca_{0.355}U_{0.210}Ti_{0.435}O_{1.645}$ heated at 1400°C in Ar.

Phase	Ca	U	Ti	O	Total
Perovskite	1.0247	0.0362	0.9391	2.9753	4.9753
Pyrochlore	1.4735	0.7966	1.7299	6.5265	10.5265
UO_2	0.3454	0.6408	0.0138	1.6546	2.6546

Table A51. Microprobe analysis of P259.

Composition $Ca_{1.35}Hf_{0.57}U_{0.08}Ti_{2.20}O_{7.05}$ heated at 1350°C in air.

Phase	Ca	Hf	U	Ti	O	Total
Perovskite	0.7814	0.1440	0.0253	1.0493	3.2312	5.2312
zirconolite-2M	1.0967	0.6075	0.1066	2.1892	6.9566	10.9566
Rutile	0.1185	0.0512	0.0043	0.8260	1.8836	2.8836

Table A52. Microprobe analysis of P260.

Composition $Ca_{1.37}Hf_{0.38}U_{0.25}Ti_{2.20}O_{7.03}$ heated at 1350°C in air.

Phase	Ca	Hf	U	Ti	O	Total
Perovskite	0.9244	0.0032	0.0048	1.0676	3.0780	5.0780
Pyrochlore	1.3255	0.2951	0.3811	1.9983	6.8650	10.8650
zirconolite-2M	1.2426	0.4022	0.2860	2.0692	6.9004	10.9004
Rutile	0.0332	0.0357	0.0026	0.9285	1.9681	2.9681

Table A53. Microprobe analysis of P261.

Composition $Ca_{1.38}Hf_{0.22}U_{0.40}Ti_{2.20}O_{7.02}$ heated at 1350°C in air.

Phase	Ca	Hf	U	Ti	O	Total
Perovskite	0.7635	0.0840	0.1074	1.0451	3.2902	5.2902
Pyrochlore	1.3569	0.2592	0.4337	1.9502	6.8600	10.8600
zirconolite-2M	1.2371	0.3746	0.3190	2.0693	6.9224	10.9224
Rutile	0.2202	0.0407	0.0508	0.6883	1.8052	2.8052

Table A54. Microprobe analysis of P262.

Composition $Ca_{1.40}Hf_{0.06}U_{0.54}Ti_{2.20}O_{7.00}$ heated at 1350°C in air.

Phase	Ca	Hf	U	Ti	O	Total
Perovskite	0.6819	0.0268	0.1507	1.1406	3.3934	5.3934
Pyrochlore	1.3797	0.0719	0.5226	2.0258	6.8816	10.8816
Rutile	0.2204	0.0161	0.0704	0.6931	1.8148	2.8148

Table A55. Microprobe analysis of P263.

Composition $Ca_{1.04}Hf_{0.82}U_{0.14}Ti_{2.40}O_{7.76}$ heated at 1350°C in air.

Phase	Ca	Hf	U	Ti	O	Total
Zirconolite-2M	1.0839	0.6200	0.1192	2.1769	6.9757	10.9757
Rutile	0.0269	0.0561	0.0052	0.9118	1.9757	2.9757

Table A56. Microprobe analysis of P264.

Composition $Ca_{1.07}Hf_{0.61}U_{0.32}Ti_{2.40}O_{7.73}$ heated at 1350°C in air.

Phase	Ca	Hf	U	Ti	O	Total
Pyrochlore	1.4161	0.2301	0.5626	1.7912	6.8652	10.8652
zirconolite-2M	1.2316	0.4901	0.3245	1.9538	6.9306	10.9306
Rutile	0.0033	0.0686	0.0042	0.9239	1.9988	2.9988

Table A57. Microprobe analysis of P265.

Composition $Ca_{1.11}Hf_{0.38}U_{0.51}Ti_{2.40}O_{7.69}$ heated at 1350ºC in air.

Phase	Ca	Hf	U	Ti	O	Total
Pyrochlore	1.3735	0.2345	0.5213	1.8707	6.8872	10.8872
zirconolite-2M	1.2556	0.4363	0.3676	1.9405	6.9282	10.9282
Rutile	0.1498	0.0654	0.0598	0.7250	1.8801	2.8801

Table A58. Microprobe analysis of P266.

Composition $Ca_{1.14}Hf_{0.17}U_{0.69}Ti_{2.40}O_{7.66}$ heated at 1350ºC in air.

Phase	Ca	Hf	U	Ti	O	Total
Pyrochlore	1.4472	0.1191	0.7167	1.7170	6.9112	10.9112
Rutile	0.1353	0.0367	0.0730	0.7550	1.9012	2.9012

Table A59. Microprobe analysis of P267.

Composition $Ca_{0.56}Hf_{1.09}U_{0.35}Ti_{2.70}O_{8.84}$ heated at 1350ºC in air.

Phase	Ca	Hf	U	Ti	O	Total
Pyrochlore	1.4309	0.2957	0.6116	1.6618	6.5691	10.5691
zirconolite-2M	1.1567	0.6436	0.3060	1.8937	6.9963	10.9963
$HfTiO_4$	0.0180	0.8106	0.0396	1.1318	4.0018	6.0018
Rutile	0.0050	0.1216	0.0107	0.8627	2.0004	3.0004

Table A60. Microprobe analysis of P268.

Composition $Ca_{0.66}Hf_{0.64}U_{0.70}Ti_{2.80}O_{8.94}$ heated at 1350ºC in air.

Phase	Ca	Hf	U	Ti	O	Total
Brannerite	0.2750	0.1261	0.6442	1.9547	6.0471	9.0471
$HfTiO_4$	0.0239	0.8150	0.0426	1.1185	3.9974	5.9974
Rutile	0.0059	0.1210	0.0173	0.8558	2.0028	3.0028

Table A61. Microprobe analysis of P269.

Composition $Ca_{0.72}Hf_{0.36}U_{0.92}Ti_{2.90}O_{9.08}$ heated at 1350ºC in air.

Phase	Ca	Hf	U	Ti	O	Total
Pyrochlore	1.4414	0.2006	0.7282	1.6298	6.9227	10.9227
brannerite	0.2654	0.1405	0.4647	2.1294	5.9670	8.9670
Rutile	0.0112	0.0805	0.0265	0.8818	2.0020	3.0020

Table A62. Microprobe analysis of P270.

Composition $Ca_{0.77}Hf_{0.13}U_{1.10}Ti_{3.00}O_{9.23}$ heated at 1350ºC in air.

Phase	Ca	Hf	U	Ti	O	Total
Pyrochlore	1.4681	0.1345	0.7083	1.6891	6.8861	10.8861
brannerite	0.2618	0.1044	0.5083	2.1255	5.9924	8.9924
Rutile	0.0006	0.0482	0.0155	0.9357	2.0072	3.0072

Table A63. Quantitative SEM/EDS analysis of L990357 [16].

Composition $CaHf_{0.5}U_{0.5}Ti_2O_7$ heated at 1400ºC in Ar.

U is assumed to be +4 in this sample.

Phase	Ca	Hf	U	Ti	O	Total
Pyrochlore	1.106	0.349	0.721	1.877	7.000	11.053
zirconolite-2M	1.068	0.538	0.533	1.895	7.000	11.034
Brannerite	0.176	0.165	0.765	1.982	6.000	9.088
$HfTiO_4$		0.798	0.055	1.147	4.000	6.000
Rutile		0.142	0.010	0.848	2.000	3.000

Table A64. Quantitative SEM/EDS analysis of L990358 [16].

Composition $CaHf_{0.4}U_{0.6}Ti_{1.9}O_{6.8}$ heated at 1400ºC in Ar.

U is assumed to be +4 in this sample.

Phase	Ca	Hf	U	Ti	O	Total
Pyrochlore	1.141	0.384	0.690	1.856	7.000	11.070
Brannerite	0.152	0.169	0.756	1.999	6.000	9.076
$HfTiO_4$		0.806	0.057	1.137	4.000	6.000

Table A65. Quantitative SEM/EDS analysis of L990369 [16].

Composition $CaHf_{0.3}U_{0.7}Ti_{2.1}O_{7.2}$ heated at 1400ºC in Ar.

U is assumed to be +4 in this sample.

Phase	Ca	Hf	U	Ti	O	Total
Pyrochlore	1.261	0.273	0.711	1.885	7.000	11.130
Brannerite	0.191	0.131	0.761	2.013	6.000	9.095
Rutile		0.108	0.009	0.882	2.000	3.000

Table A66. Microprobe analysis of P285.

Composition $Ca_{0.99}Hf_{0.28}U_{0.49}Gd_{0.24}Ti_{2.50}O_{7.89}$ heated at 1350ºC in air.

Phase	Ca	Hf	U	Gd	Ti	O	Total
Pyrochlore	1.1564	0.2218	0.3863	0.2887	1.9468	6.8924	10.8924
zirconolite-4M	1.0146	0.4198	0.2342	0.2523	2.0791	6.9764	10.9764
Rutile	0.0508	0.0599	0.0158	0.0099	0.8636	1.9522	2.9522

Table A67. Microprobe analysis of P288.

Composition $Ca_{0.96}Hf_{0.68}U_{0.28}Gd_{0.08}Ti_{2.16}O_{7.32}$ heated at 1350ºC in air.

Phase	Ca	Hf	U	Gd	Ti	O	Total
zirconolite-4M	1.0920	0.6377	0.2832	0.0830	1.9041	7.0081	11.0081
Rutile	0.0535	0.1226	0.0192	0.0012	0.8035	1.9555	2.9555

Table A68. Microprobe analysis of P289.

Composition $Ca_{0.85}Hf_{0.67}U_{0.18}Gd_{0.30}Ti_{2.16}O_{7.32}$ heated at 1350ºC in air.

Phase	Ca	Hf	U	Gd	Ti	O	Total
zirconolite-4M	0.9291	0.5979	0.1823	0.2925	1.9982	7.0158	11.0158
zirconolite-2M	0.8788	0.7139	0.1414	0.2797	1.9862	7.0520	11.0520
Rutile	0.0929	0.1525	0.0096	0.0208	0.7242	1.9015	2.9015

Table A69. Microprobe analysis of P290.

Composition $Ca_{0.95}Hf_{0.40}U_{0.55}Gd_{0.10}Ti_{2.16}O_{7.32}$ heated at 1350ºC in air.

Phase	Ca	Hf	U	Gd	Ti	O	Total
pyrochlore	1.3145	0.2688	0.6246	0.1390	1.6531	6.9283	10.9283
zirconolite-4M	1.2490	0.4066	0.5282	0.0874	1.7288	6.9714	10.9714
zirconolite-2M	0.5535	1.0970	0.3385	0.0595	1.9515	7.5860	11.5860
Rutile	0.0088	0.1418	0.0158	0.0000	0.8336	1.9991	2.9991

Table A70. Microprobe analysis of P291.

Composition $Ca_{0.82}Hf_{0.41}U_{0.41}Gd_{0.36}Ti_{2.16}O_{7.32}$ heated at 1350ºC in air.

Phase	Ca	Hf	U	Gd	Ti	O	Total
pyrochlore	0.9557	0.3480	0.4436	0.3692	1.8835	7.0815	11.0815
zirconolite-4M	0.9854	0.4469	0.3614	0.3422	1.8641	7.0242	11.0242
Rutile	0.0354	0.1192	0.0252	0.0115	0.8087	1.9714	2.9714

Table A71. Microprobe analysis of P292.

Composition $Ca_{0.54}Hf_{0.45}U_{0.09}Gd_{0.92}Ti_{2.16}O_{7.32}$ heated at 1350ºC in air.

Phase	Ca	Hf	U	Gd	Ti	O	Total
pyrochlore	0.5179	0.3621	0.0855	1.0231	2.0114	7.0133	11.0133
zirconolite-4M	0.5452	0.4454	0.0689	0.8735	2.0670	7.0525	11.0242
Rutile	0.0491	0.0853	0.0076	0.0860	0.7720	1.9117	2.9117

Table A72. Quantitative SEM/EDS analysis of L990354 [16].

Composition $Ca_{0.75}Hf_{0.5}U_{0.25}Gd_{0.5}Ti_{2.1}O_{7.2}$ heated at 1400ºC in Ar.

U is assumed to be +4 in this sample.

Phase	Ca	Hf	U	Gd	Ti	O	Total
Pyrochlore	0.722	0.327	0.366	0.633	1.946	7.000	11.044
zirconolite-4M	0.760	0.534	0.212	0.489	2.006	7.000	11.002
Rutile		0.105	0.005		0.890	2.000	3.000

Table A73. Quantitative SEM/EDS analysis of L990367 [16].

Composition $Ca_{0.7}Hf_{0.4}U_{0.3}Gd_{0.6}Ti_2O_7$ heated at 1400ºC in Ar.

U is assumed to be +4 in this sample.

Phase	Ca	Hf	U	Gd	Ti	O	Total
Pyrochlore	0.711	0.324	0.317	0.683	1.991	7.000	11.026
zirconolite-4M	0.708	0.527	0.220	0.569	1.973	7.000	10.996
Rutile		0.110	0.004		0.886	2.000	3.000

Table A74. Quantitative SEM/EDS analysis of L990368 [16].

Composition $Ca_{0.75}Hf_{0.3}U_{0.35}Gd_{0.7}Ti_2O_7$ heated at 1400ºC in Ar.

U is assumed to be +4 in this sample.

Phase	Ca	Hf	U	Gd	Ti	O	Total
Pyrochlore	0.711	0.278	0.290	0.753	2.012	7.000	11.044
zirconolite-4M	0.734	0.470	0.162	0.594	2.055	7.000	11.016
Rutile		0.079	0.003		0.918	2.000	3.000

Table A75. Quantitative SEM/EDS analysis of R97m030-3B [11].

Composition $Ca_{0.81}Hf_{0.23}Ce_{0.20}U_{0.40}Gd_{0.20}Ga_{0.06}Al_{0.02}Mg_{0.04}Ti_{2.04}O_7$ heated at 1350ºC in Ar.

Ce is assumed to be +4 in this sample.

Phase	Ca	Hf	Ce	U	Gd	Ga	Al	Mg	Ti	O	Total
Pyrochlore	0.90	0.18	0.22	0.45	0.21				2.05	7.00	11.01
zirconolite-2M	0.63	0.66	0.11	0.15	0.17	0.36	0.09	0.07	1.77	7.00	11.01
zirconolite-2M	0.55	0.44	0.15	0.15	0.15	0.46	0.11	0.04	1.93	7.00	10.98
Rutile		0.05		0.01		0.01	0.01		0.93	2.00	3.01

Table A76. Quantitative SEM/EDS analysis of R97m030-5B [11].

Composition $Ca_{0.81}Hf_{0.23}Ce_{0.20}U_{0.40}Gd_{0.20}Al_{0.01}Mg_{0.09}Ti_{2.06}O_7$ heated at 1350ºC in Ar.

Ce is assumed to be +4 in this sample.

Phase	Ca	Hf	Ce	U	Gd	Al	Mg	Ti	O	Total
Pyrochlore	0.84	0.26	0.24	0.44	0.18	0.03	0.04	1.96	7.00	10.99
Rutile		0.08		0.01				0.91	2.00	3.00

Table A77. Quantitative SEM/EDS analysis of R97m030-7B [11].

Composition $Ca_{0.84}Hf_{0.23}Ce_{0.20}U_{0.41}Gd_{0.20}Al_{0.03}Mg_{0.02}Ti_{2.08}O_{7.04}$ heated at 1350ºC in Ar.
Ce is assumed to be +4 in this sample.

Phase	Ca	Hf	Ce	U	Gd	Al	Mg	Ti	O	Total
Pyrochlore	0.86	0.27	0.20	0.46	0.20	0.04	0.05	1.93	7.00	11.01
rutile		0.08		0.01				0.91	2.00	3.00

Table A78. Quantiative SEM/EDS analysis of R97m030-8B [11].

Composition $Ca_{0.83}Hf_{0.19}Ce_{0.17}U_{0.33}Gd_{0.17}Al_{0.14}Mg_{0.16}K_{0.10}Na_{0.07}Si_{0.11}Ti_{1.70}O_{6.6}$ with minor amounts of oxides of B, Fe, Cr, Ni, Mo, Ta and W, heated at 1350ºC in Ar.

Phase	Ca	Hf	Ce	U	Gd	Al	Na	Ti	O	Total
Perovskite	0.62	0.01	0.18	0.01	0.05	0.04	0.09	0.94	3.00	4.94

Table A79. Microprobe analysis of Ryerson 1/4 [13].

Composition $Ca_{0.84}Hf_{0.24}Ce_{0.21}U_{0.42}Gd_{0.21}Ti_{2.08}O_{7.06}$ heated at 1350ºC in $f(O_2) = 10^{-2.6}$ atm.

Phase	Ca	Hf	Ce	U	Gd	Al	Ti	O	Total
Pyrochlore	0.968	0.221	0.243	0.395	0.238	0.024	1.911	6.800	10.800
Brannerite	0.081	0.115	0.208	0.498	0.136	0.033	1.930	5.732	8.732
Rutile	0.002	0.076	0.000	0.008	0.001	0.010	0.903	1.992	2.992

Table A80. Microprobe analysis of Ryerson 1/5 [13].

Composition $Ca_{0.84}Hf_{0.24}Ce_{0.21}U_{0.42}Gd_{0.21}Ti_{2.08}O_{7.06}$ heated at 1350ºC in $f(O_2) = 10^{-5.05}$ atm.

Phase	Ca	Hf	Ce	U	Gd	Al	Ti	O	Total
Pyrochlore	0.888	0.216	0.237	0.407	0.225	0.011	2.016	6.875	10.875
Rutile	0.002	0.066	0.001	0.005	0.001	0.007	0.918	1.993	2.993

Table A81. Microprobe analysis of Ryerson 7/4 [13].

Composition $Ca_{0.83}Hf_{0.24}Ce_{0.21}U_{0.41}Gd_{0.21}Ti_{2.10}O_{7.06}$ with 10 wt % Al_2O_3 heated at 1350ºC in $f(O_2) = 10^{-2.6}$ atm.

Phase	Ca	Hf	Ce	U	Gd	Al	Ti	O	Total
Pyrochlore	1.005	0.146	0.223	0.417	0.231	0.018	1.961	6.760	10.760
zirconolite-2M	0.744	0.634	0.096	0.153	0.181	0.350	1.843	6.943	10.943
Brannerite	0.071	0.080	0.205	0.526	0.131	0.075	1.912	5.723	8.723
rutile	0.002	0.049	0.001	0.010	0.000	0.018	0.920	1.988	2.988

Table A82. Microprobe analysis of Ryerson 7/5 [13].

Composition $Ca_{0.83}Hf_{0.24}Ce_{0.21}U_{0.41}Gd_{0.21}Ti_{2.10}O_{7.06}$ with 10 wt % Al_2O_3 heated at 1350ºC in $f(O_2) = 10^{-5.05}$ atm.

Phase	Ca	Hf	Ce	U	Gd	Al	Ti	O	Total
Pyrochlore	0.911	0.161	0.218	0.448	0.226	0.027	2.009	6.853	10.853
zirconolite-2M	0.715	0.673	0.093	0.132	0.161	0.353	1.871	6.981	10.981
Brannerite	0.044	0.081	0.161	0.619	0.100	0.055	1.940	5.798	8.798
rutile	0.002	0.045	0.000	0.006	0.000	0.012	0.935	1.992	2.992

Table A83. Quantitative SEM/EDS analysis of L990381 [16].
Composition $CaHf_{0.5}Th_{0.5}Ti_2O_7$ heated at 1400ºC in air.

Phase	Ca	Hf	Th	Ti	O	Total
zirconolite-4M	1.018	0.465	0.582	1.944	7.000	11.009
zirconolite-2M	0.990	0.774	0.221	2.009	7.000	10.994
perovskite	0.801	0.018	0.097	0.986	3.000	4.902

Table A84. Quantitative SEM/EDS analysis of L990382 [16].
Composition $CaHf_{0.3}Th_{0.7}Ti_{2.1}O_{7.2}$ heated at 1400ºC in air.

Phase	Ca	Hf	Th	Ti	O	Total
Pyrochlore	0.987	0.381	0.702	1.924	7.000	10.994
Pyrochlore	0.986	0.379	0.696	1.932	7.000	10.993

Table A85. Quantitative SEM/EDS analysis of L990383 [16].
Composition $CaHf_{0.3}Th_{0.7}Ti_{2.1}O_{7.2}$ heated at 1400ºC in air.

Phase	Ca	Hf	Th	Ti	O	Total
Pyrochlore	1.004	0.282	0.712	2.003	7.000	11.001
Brannerite		0.138	0.918	1.943	6.000	8.999
ThO_2		0.007	0.985	0.009	2.000	3.001

Table A86. Quantitative SEM/EDS analysis of L990389 [16].
Composition $CaHf_{0.3}Th_{0.7}Ti_{2.1}O_{7.2}$ heated at 1300ºC in air.

Phase	Ca	Hf	Th	Ti	O	Total
Pyrochlore	1.024	0.332	0.692	1.965	7.000	11.013
Brannerite		0.152	0.922	1.926	6.000	9.000
Perovskite	0.797	0.016	0.103	0.983	3.000	4.899
ThO_2		0.007	0.952	0.042	2.000	3.001

Table A87. Microprobe analysis of P300.
Composition $Ca_{1.5}Hf_{0.34}Th_{0.16}Ti_{2.3}O_{7.1}$ heated at 1350ºC in air.

Phase	Ca	Hf	Th	Ti	O	Total
Pyrochlore	0.6002	0.3929	0.6359	2.3710	7.3998	11.3998
Brannerite	0.1979	0.2492	0.6683	1.8846	5.8021	8.8021
Perovskite	0.7960	0.0769	0.0697	1.0574	3.2040	5.2040
zirconolite-2M	1.0797	0.5692	0.1406	2.2105	6.9203	10.9203
Rutile	0.0413	0.0567	0.0040	0.8980	1.9587	2.9587

Table A88. Microprobe analysis of P301.

Composition $Ca_{1.5}Hf_{0.15}Th_{0.35}Ti_{2.3}O_{7.1}$ heated at 1350°C in air.

Phase	Ca	Hf	Th	Ti	O	Total
Pyrochlore	0.8417	0.2239	0.6495	2.2849	7.1583	11.1583
Brannerite	0.1529	0.1801	0.7486	1.9184	5.8471	8.8471
Perovskite	0.8480	0.0305	0.1120	1.0095	3.1520	5.1520
zirconolite-2M	1.0958	0.3352	0.3008	2.2682	6.9042	10.9042
Rutile	0.1270	0.0555	0.0580	0.7595	1.8730	2.8730

Table A89. Microprobe analysis of P302.

Composition $Ca_{1.04}Hf_{0.72}Th_{0.24}Ti_{2.3}O_{7.56}$ heated at 1350°C in air.

Phase	Ca	Hf	Th	Ti	O	Total
Pyrochlore	0.5462	0.4828	0.5844	2.3866	7.4538	11.4538
Brannerite	0.2077	0.2851	0.6379	1.8693	5.7923	8.7923
Perovskite	0.7154	0.1378	0.0771	1.0697	3.2846	5.2846
zirconolite-2M	0.8963	0.5949	0.3005	2.2083	7.1037	11.1037

Table A90. Microprobe analysis of P303.

Composition $Ca_{1.10}Hf_{0.34}Th_{0.56}Ti_{2.3}O_{7.5}$ heated at 1350°C in air.

Phase	Ca	Hf	Th	Ti	O	Total
Pyrochlore	1.0158	0.3513	0.5480	2.0849	6.9842	10.9842
Brannerite	0.2053	0.2345	0.7269	1.8333	5.7947	8.7947
Perovskite	0.6870	0.0747	0.1632	1.0751	3.3130	5.3130
zirconolite-2M	1.0133	0.4531	0.3419	2.1917	6.9867	10.9867

Table A91. Microprobe analysis of P304.

Composition $Ca_{0.66}Hf_{1.18}Th_{0.16}Ti_{2.4}O_{8.14}$ heated at 1350°C in air.

Phase	Ca	Hf	Th	Ti	O	Total
Brannerite	0.0218	0.2674	0.7577	1.9531	5.9782	8.9782
zirconolite-2M	0.8447	0.9290	0.1526	2.0737	7.1553	11.1553
$HfTiO_4$	0.0864	0.5505	0.1818	1.1813	3.9136	5.9136
Rutile	0.0766	0.1844	0.0218	0.7172	1.9234	2.9234

Table A92. Microprobe analysis of P305.

Composition $Ca_{0.66}Hf_{0.68}Th_{0.66}Ti_{2.8}O_{8.94}$ heated at 1350°C in air.

Phase	Ca	Hf	Th	Ti	O	Total
Pyrochlore	0.3515	0.3631	0.7996	2.4858	7.6485	11.6485
Brannerite	0.0705	0.1960	0.7990	1.9345	5.9295	8.9295
zirconolite-2M	0.7208	0.6014	0.3384	2.3394	7.2792	11.2792

Table A93. Microprobe analysis of P306.

Composition $Ca_{0.72}Hf_{0.20}Th_{1.08}Ti_{3.3}O_{9.88}$ heated at 1350ºC in air.

Phase	Ca	Hf	Th	Ti	O	Total
Pyrochlore	0.7696	0.1878	0.6260	2.4166	7.2304	11.2304
Brannerite	0.0218	0.1536	0.8525	1.9721	5.9782	8.9782
Rutile	0.0030	0.0482	0.1601	0.7887	1.9970	2.9970

Table A94. Quantitative SEM/EDS analysis of L990378 [16].

Composition $Ca_{0.75}Hf_{0.5}Th_{0.25}Gd_{0.5}Ti_{2.1}O_{7.2}$ heated at 1400ºC in air.

Phase	Ca	Hf	Th	Gd	Ti	O	Total
Pyrochlore	0.706	0.369	0.317	0.585	2.023	7.000	11.000
zirconolite-4M	0.736	0.543	0.148	0.459	2.097	7.000	10.983
Rutile		0.093			0.907	2.000	3.000

Table A95. Quantitative SEM/EDS analysis of L990379 [16].

Composition $Ca_{0.7}Hf_{0.4}Th_{0.3}Gd_{0.6}Ti_2O_7$ heated at 1400ºC in air.

Phase	Ca	Hf	Th	Gd	Ti	O	Total
Pyrochlore	0.686	0.345	0.284	0.657	2.034	7.000	11.006
zirconolite-4M	0.726	0.527	0.124	0.501	2.111	7.000	10.989
Rutile		0.085			0.915	2.000	3.000

Table A96. Quantitative SEM/EDS analysis of L990380 [16].

Composition $Ca_{0.75}Hf_{0.3}Th_{0.35}Gd_{0.7}Ti_{1.9}O_{6.9}$ heated at 1400ºC in air.

Phase	Ca	Hf	Th	Gd	Ti	O	Total
Pyrochlore	0.683	0.305	0.251	0.727	2.057	7.000	11.023
Perovskite	0.693	0.008	0.034	0.160	0.991	3.000	4.886

Table A97. Quantitative SEM/EDS analysis of L990388 [16].

Composition $Ca_{0.75}Hf_{0.3}Th_{0.35}Gd_{0.7}Ti_{1.9}O_{6.9}$ heated at 1300ºC in air.

Phase	Ca	Hf	Th	Gd	Ti	O	Total
Pyrochlore	0.671	0.290	0.271	0.746	2.044	7.000	11.022
zirconolite-4M	0.739	0.442	0.151	0.587	2.097	7.000	11.016
Perovskite	0.607	0.034	0.046	0.179	0.982	3.000	4.848

Table A98. Microprobe analysis of Ryerson 8/1 [17].

Composition $Ca_{0.87}Hf_{0.25}Th_{0.23}U_{0.43}Gd_{0.22}Ti_{2.21}O_{7.66}$ heated at 1350ºC in air.

Phase	Ca	Hf	Th	U	Gd	Al	Ti	O	Total
Pyrochlore	1.127	0.207	0.140	0.399	0.217	0.021	1.890	6.955	10.956
zirconolite-2M	0.917	0.830	0.021	0.072	0.115	0.085	1.961	7.021	11.022
Brannerite	0.104	0.127	0.350	0.307	0.133	0.000	1.979	5.983	8.983
rutile	0.002	0.072	0.000	0.004	0.000	0.010	0.911	1.993	2.992

Table A99. Microprobe analysis of Ryerson 8/2 [17].

Composition $Ca_{0.87}Hf_{0.25}Th_{0.23}U_{0.43}Gd_{0.22}Ti_{2.21}O_{7.66}$ heated at 1350ºC in air.

Phase	Ca	Hf	Th	U	Gd	Al	Ti	O	Total
Pyrochlore	1.126	0.236	0.143	0.345	0.213	0.000	1.938	6.942	10.943
Brannerite	0.124	0.141	0.315	0.303	0.136	0.000	1.980	5.957	8.957
rutile	0.000	0.077	0.000	0.003	0.000	0.000	0.920	2.001	3.001

Table A100. Microprobe analysis of Ryerson 8/3 [13].

Composition $Ca_{0.87}Hf_{0.25}Th_{0.23}U_{0.43}Gd_{0.22}Ti_{2.21}O_{7.66}$ heated at 1350ºC in air.

Phase	Ca	Hf	Th	U	Gd	Al	Ti	O	Total
Pyrochlore	1.118	0.232	0.143	0.380	0.218	0.000	1.909	6.963	10.963
Brannerite	0.097	0.144	0.334	0.320	0.129	0.003	1.974	5.999	9.000
rutile	0.001	0.083	0.000	0.005	0.001	0.005	0.904	1.996	2.996

Table A101. Quantitative SEM/EDS analysis of mws980268 [18].

Composition $Ca_{0.99}Hf_{0.24}Th_{0.21}U_{0.36}Gd_{0.20}Ti_{2.09}O_{7.09}$ heated at 1350ºC in air.

U is assumed to be +4 in this sample.

Phase	Ca	Hf	Th	U	Gd	Ti	O	Total
Pyrochlore	1.06	0.27	0.21	0.37	0.19	1.97	7.00	11.07
Brannerite	0.08	0.15	0.47	0.27	0.10	1.98	6.00	9.05

Table A102. Quantitative SEM/EDS analysis of mws980286 [18].

Composition $Ca_{0.99}Hf_{0.24}Th_{0.21}U_{0.36}Gd_{0.20}Ti_{2.09}O_{7.09}$ heated at 1350ºC in air.

U is assumed to be +4 in this sample.

Phase	Ca	Hf	Th	U	Gd	Ti	O	Total
Pyrochlore	1.07	0.25	0.19	0.37	0.21	1.99	7.00	11.08
Brannerite	0.09	0.14	0.48	0.28	0.10	1.98	6.00	9.07
Rutile	0.005	0.10	0.002	0.002		0.89	2.00	3.00

Table A103. Quantitative SEM/EDS analysis of mws980288 [18].

Composition $Ca_{0.99}Hf_{0.24}Th_{0.21}U_{0.36}Gd_{0.20}Ti_{2.09}O_{7.09}$ heated at 1350ºC in air.

U is assumed to be +4 in this sample.

Phase	Ca	Hf	Th	U	Gd	Ti	O	Total
Pyrochlore	1.05	0.25	0.16	0.41	0.24	1.98	7.00	11.09
Brannerite	0.09	0.14	0.46	0.30	0.10	1.98	6.00	9.07
zirconolite-4M	0.91	0.47	0.05	0.26	0.19	2.12	7.00	11.00
Rutile	0.004	0.06	0.001	0.004		0.94	2.00	3.01

Table A104. Microprobe analysis of Ryerson 8/6 [13].

Composition $Ca_{0.87}Hf_{0.25}Th_{0.23}U_{0.43}Gd_{0.22}Ti_{2.21}O_{7.66}$ heated at 1350ºC with $f_{O2} = 10^{-5.90}$ atm..

Phase	Ca	Hf	Th	U	Gd	Al	Ti	O	Total
Pyrochlore	0.999	0.226	0.166	0.359	0.225	0.006	2.019	6.886	10.886
Brannerite	0.052	0.118	0.358	0.403	0.084	0.014	1.971	5.899	8.899
zirconolite-2M	0.941	0.835	0.022	0.061	0.102	0.134	1.903	6.937	10.935
rutile	0.001	0.062	0.000	0.003	0.000	0.002	0.933	2.000	3.001

Table A105. Microprobe analysis of Ryerson 8/7 [13].

Composition $Ca_{0.87}Hf_{0.25}Th_{0.23}U_{0.43}Gd_{0.22}Ti_{2.21}O_{7.66}$ heated at 1350 ºC with $f_{O2} = 10^{-8.00}$ atm.

Phase	Ca	Hf	Th	U	Gd	Al	Ti	O	Total
Pyrochlore	0.953	0.236	0.189	0.365	0.218	0.010	2.030	6.935	10.936
Brannerite	0.019	0.127	0.371	0.441	0.057	0.014	1.971	5.946	8.946
rutile	0.000	0.060	0.000	0.001	0.000	0.004	0.935	1.998	2.998

Table A106. Microprobe analysis of Ryerson 8/8 [13].

Composition $Ca_{0.87}Hf_{0.25}Th_{0.23}U_{0.43}Gd_{0.22}Ti_{2.21}O_{7.66}$ heated at 1350ºC with $f_{O2} = 10^{-10.06}$ atm.

Phase	Ca	Hf	Th	U	Gd	Al	Ti	O	Total
Pyrochlore	0.914	0.236	0.198	0.379	0.213	0.009	2.051	6.975	10.975
Brannerite	0.012	0.125	0.383	0.466	0.034	0.008	1.972	5.967	8.967
zirconolite-2M	0.786	0.724	0.045	0.081	0.130	0.157	2.077	7.070	11.070
rutile	0.000	0.062	0.000	0.000	0.000	0.006	0.931	1.995	2.994

Table A107. Microprobe analysis of Ryerson 8/9 [13].

Composition $Ca_{0.87}Hf_{0.25}Th_{0.23}U_{0.43}Gd_{0.22}Ti_{2.21}O_{7.66}$ heated at 1350ºC with $f_{O2} = 10^{-6.83}$ atm.

Phase	Ca	Hf	Th	U	Gd	Al	Ti	O	Total
Pyrochlore	0.976	0.239	0.179	0.353	0.213	0.008	2.031	6.912	10.911
Brannerite	0.041	0.129	0.351	0.419	0.072	0.016	1.972	5.915	8.915
zirconolite-2M	0.930	0.792	0.026	0.063	0.113	0.164	1.912	6.932	10.932
rutile	0.001	0.062	0.000	0.002	0.000	0.004	0.932	1.999	3.000

Table A108. Quantitative SEM/EDS analysis of R00m026 (90%$CaPuTi_2O_7$+10%$CaTiO_3$) [12].
Composition $Ca_{1.17}Pu_{0.83}Ti_2O_{6.83}$ heated at 1300ºC in air.

Phase	Ca	Pu	Ti	O	Total
Pyrochlore	0.95	0.96	2.07	7.00	10.98
Perovskite	0.93	0.04	1.00	3.00	4.97

Table A109. Quantitative SEM/EDS analysis of R00m026 (90%$CaPuTi_2O_7$+10%TiO_2) [12].
Composition $Ca_{0.855}Pu_{0.855}Ti_{2.29}O_{7.145}$ heated at 1300ºC in air.

Phase	Ca	Pu	Ti	O	Total
Pyrochlore	0.95	0.96	2.07	7.00	10.98
Perovskite	0.93	0.04	1.00	3.00	4.97
Rutile			1.00	2.00	3.00

Table A110. Quantitative SEM/EDS analysis of Pu08202A [15].
Composition $PuTi_2O_6$ heated at 1550ºC in air.

Phase	Ca	Pu	Ti	O	Total
Brannerite		1.015	1.985	6.00	9.000
PuO_2		1.000	0.000	2.00	3.000
Rutile		0.001	0.999	2.00	3.000

Table A111. Quantitative SEM/EDS analysis of Pu12402A [15].
Composition $CaPuTi_2O_7$ heated at 1525ºC in air.

Phase	Ca	Pu	Ti	O	Total
Pyrochlore	0.96	0.95	2.065	7.00	10.975
Perovskite	0.885	0.06	0.995	3.00	4.94
PuO_2		1.00		2.00	3.00
Rutile	0.001	0.0005	1.00	2.00	3.002

Table A112. Quantitative SEM/EDS analysis of Pu12501A [15].
Composition $Pu_{0.69}Ti_{2.31}O_6$ heated at 1550ºC in air.

Phase	Ca	Pu	Ti	O	Total
Brannerite		1.00	1.99	6.00	8.99
PuO_2		1.00		2.00	3.00
Rutile		0.001	0.999	2.00	3.000

Table A113. Quantitative SEM/EDS analysis of Pu12502A [15].
Composition $Pu_{0.69}Ti_{2.31}O_6$ heated at 1525ºC in air.

Phase	Ca	Pu	Ti	O	Total
Brannerite		0.996	2.00	6.00	8.996
PuO_2		1.00		2.00	3.00
Rutile		0.001	0.999	2.00	3.000

Table A114. Quantitative SEM/EDS analysis of Pu12901A [15].
Composition $Ca_{0.94}Pu_{0.94}Ti_{2.12}O_{7.06}$ heated at 1490ºC in air.

Phase	Ca	Pu	Ti	O	Total
Pyrochlore	0.93	0.95	2.08	7.00	10.96
PuO_2	0.0035	1.00		2.00	3.004
Rutile	0.005	0.003	0.995	2.00	3.003

Table A115. Quantitative SEM/EDS analysis of Pu11501A [16].
Composition $CaHf_{0.5}Pu_{0.5}Ti_2O_7$ heated at 1400ºC in Ar.

Phase	Ca	Hf	Pu	Ti	O	Total
Pyrochlore	0.971	0.380	0.706	1.928	7.000	10.986
zirconolite-4M	0.952	0.572	0.487	1.965	7.000	10.976
Perovskite	0.865	0.016	0.061	0.990	3.000	4.932

Table A116. Quantitative SEM/EDS analysis of Pu11601A [16].
Composition $CaHf_{0.4}Pu_{0.6}Ti_{1.9}O_{6.8}$ heated at 1400ºC in Ar.

Phase	Ca	Hf	Pu	Ti	O	Total
Pyrochlore	0.909	0.234	0.787	2.024	7.000	10.954
zirconolite-2M	0.922	0.700	0.228	2.111	7.000	10.961
Rutile		0.062	0.003	0.935	2.000	3.000

Table A117. Quantitative SEM/EDS analysis of Pu11701A [16].
Composition $CaHf_{0.3}Pu_{0.7}Ti_{2.1}O_{7.2}$ heated at 1400ºC in Ar.

Phase	Ca	Hf	Pu	Ti	O	Total
Pyrochlore	0.951	0.379	0.710	1.936	7.000	10.975
zirconolite-4M	0.953	0.499	0.563	1.961	7.000	10.976

Table A118. Microprobe analysis of ME3730.

Composition $Ca_{0.86}Hf_{0.90}Pu_{0.24}Ti_{2.70}O_{8.54}$ heated at 1350ºC in air.

Phase	Ca	Hf	Pu	Ti	O	Total
Pyrochlore	0.9544	0.4020	0.6933	1.9503	7.0456	11.0456
zirconolite-4M	0.9428	0.6135	0.4780	1.9657	7.0572	11.0572
zirconolite-2M	0.9315	0.8645	0.1550	2.0490	7.0685	11.0685
PuO_2	0.0000	0.0520	0.9381	0.0099	2.0000	3.0000
Rutile	0.0051	0.1340	0.0023	0.8587	1.9951	2.9952

Table A119. Microprobe analysis of ME3732.

Composition $Ca_{0.92}Hf_{0.26}Pu_{0.82}Ti_{3.50}O_{10.08}$ heated at 1350ºC in air.

Phase	Ca	Hf	Pu	Ti	O	Total
Pyrochlore	0.9705	0.1711	0.7568	2.1016	7.0295	11.0295
Rutile	0.0033	0.0481	0.0019	0.9467	1.9967	2.9967

Table A120. Quantitative SEM/EDS analysis of Pu11201A [16].

Composition $Ca_{0.75}Hf_{0.5}Pu_{0.25}Gd_{0.5}Ti_{2.1}O_{7.2}$ heated at 1400ºC in Ar.

Phase	Ca	Hf	Pu	Gd	Ti	O	Total
Pyrochlore	0.643	0.308	0.357	0.659	2.019	7.000	10.986
zirconolite-4M	0.719	0.504	0.192	0.500	2.069	7.000	10.985
Rutile		0.081	0.000		0.919	2.000	3.000

Table A121. Quantitative SEM/EDS analysis of Pu11301A [16].

Composition $Ca_{0.7}Hf_{0.4}Pu_{0.3}Gd_{0.6}Ti_2O_7$ heated at 1400ºC in Ar.

Phase	Ca	Hf	Pu	Gd	Ti	O	Total
Pyrochlore	0.653	0.299	0.321	0.713	2.019	7.000	11.005
zirconolite-4M	0.666	0.447	0.204	0.548	2.105	7.000	10.970
Rutile		0.070	0.000		0.930	2.000	3.000

Table A122. Quantitative SEM/EDS analysis of Pu11401A [16].

Composition $Ca_{0.71}Hf_{0.29}Pu_{0.33}Gd_{0.67}Ti_{1.81}O_{6.58}$ heated at 1400ºC in Ar.

Phase	Ca	Hf	Pu	Gd	Ti	O	Total
Pyrochlore	0.645	0.346	0.269	0.722	2.021	7.000	11.003
zirconolite-4M	0.717	0.512	0.133	0.568	2.071	7.000	11.001
Perovskite	0.738	0.006	0.010	0.179	0.981	3.000	4.914

Table A123. Quantitative SEM/EDS analysis of Pu12301A [19].

Composition $Ca_{0.65}Hf_{0.3}Pu_{0.35}Gd_{0.7}Ti_{1.9}O_{6.8}$ heated at 1400ºC in Ar.

Phase	Ca	Hf	Pu	Gd	Ti	O	Total
Pyrochlore	0.596	0.328	0.325	0.865	1.900	7.000	11.014
Perovskite	0.730	0.013	0.019	0.169	0.976	3.000	4.907

Table A124. Quantiative SEM/EDS analysis of Pu12302A [19].

Composition $Ca_{0.65}Hf_{0.3}Pu_{0.35}Gd_{0.7}Ti_{1.9}O_{6.8}$ heated at 1400ºC in air.

Phase	Ca	Hf	Pu	Gd	Ti	O	Total
Pyrochlore	0.596	0.315	0.327	0.854	1.920	7.000	11.012
Perovskite	0.737	0.011	0.006	0.174	0.984	3.000	4.912

Table A125. Microprobe analysis of ME3679Q.

Composition $Ca_{0.89}Hf_{0.25}Pu_{0.22}U_{0.44}Gd_{0.22}Ti_{2.25}O_{7.55}$ heated at 1350ºC in air.

Phase	Ca	Hf	Pu	U	Gd	Ga	Al	Ti	O	Total
Pyrochlore	1.019	0.214	0.184	0.401	0.220	0.004	0.000	1.959	7.071	11.072
Brannerite	0.079	0.120	0.208	0.395	0.152	0.004	0.002	2.041	6.041	9.042

Table A126. Microprobe analysis of ME3680Q.

Composition $Ca_{0.89}Hf_{0.25}Pu_{0.22}U_{0.44}Gd_{0.22}Ti_{2.25}O_{7.55}$ heated at 1350ºC in air.

Phase	Ca	Hf	Pu	U	Gd	Ga	Al	Ti	O	Total
Pyrochlore	1.016	0.222	0.186	0.400	0.217	0.003	0.000	1.957	7.076	11.077
Brannerite	0.081	0.118	0.196	0.407	0.154	0.003	0.001	2.040	6.043	9.043

Table A127. Microprobe analysis of ME3688A.

Composition $Ca_{1.07}Hf_{0.26}Pu_{0.23}U_{0.35}Gd_{0.21}Ti_{2.25}O_{7.56}$ heated at 1350ºC in air.

Phase	Ca	Hf	Pu	U	Gd	Ga	Al	Ti	O	Total
Pyrochlore	1.162	0.268	0.196	0.450	0.182	0.003	0.000	1.739	6.971	10.971
Perovskite	0.881	0.014	0.008	0.004	0.056	0.002	0.008	1.026	3.086	5.085

Table A128. Quantitative SEM/EDS analysis of R97m030(1325ºC Wet Mill-Air) [11].

Composition $Ca_{0.89}Hf_{0.26}Pu_{0.22}U_{0.44}Gd_{0.22}Ti_{2.23}O_{7.52}$ heated at 1325ºC in air.

U is assumed to be +4 in this sample.

Phase	Ca	Hf	Pu	U	Gd	Al	Ti	O	Total
Pyrochlore	1.02	0.26	0.26	0.46	0.18		1.87	7.00	11.05
Brannerite	0.12	0.12	0.21	0.52	0.14		1.99	6.00	9.10
PuO_2	0.15	0.05	0.31	0.49	0.08		0.01	2.00	3.09
Rutile		0.10		0.01			0.88	2.00	2.99

Table A129. Quantitative SEM/EDS analysis of R97m030(1325ºC Dry Mill-Air) [11].
Composition $Ca_{0.89}Hf_{0.26}Pu_{0.22}U_{0.44}Gd_{0.22}Ti_{2.23}O_{7.52}$ heated at 1325ºC in air.
U is assumed to be +4 in this sample.

Phase	Ca	Hf	Pu	U	Gd	Al	Ti	O	Total
pyrochlore	0.97	0.26	0.27	0.44	0.22	0.05	1.85	7.00	11.06
zirconolite-2M	0.77	0.75	0.17	0.14	0.16	0.15	1.88	7.00	11.02
brannerite	0.11	0.12	0.21	0.48	0.17	0.08	1.96	6.00	9.13
PuO_2	0.13	0.01	0.43	0.50				2.00	3.07
rutile		0.11		0.02			0.87	2.00	3.00

Table A130. Quantitative SEM/EDS analysis of R97m030(1400ºC Wet Mill-Air) [11].
Composition $Ca_{0.89}Hf_{0.26}Pu_{0.22}U_{0.44}Gd_{0.22}Ti_{2.23}O_{7.52}$ heated at 1400ºC in air.
U is assumed to be +4 in this sample.

Phase	Ca	Hf	Pu	U	Gd	Al	Ti	O	Total
Pyrochlore	1.01	0.27	0.26	0.43	0.22	0.03	1.85	7.00	11.07
Brannerite	0.09	0.13	0.24	0.47	0.14	0.04	1.96	6.00	9.10
PuO_2	0.06	0.05	0.34	0.27	0.06	0.02	0.26	2.00	3.06
Rutile		0.10		0.01			0.89	2.00	3.00

Table A131. Quantitative SEM/EDS analysis of R97m030(1400ºC Dry Mill-Air) [11].
Composition $Ca_{0.89}Hf_{0.26}Pu_{0.22}U_{0.44}Gd_{0.22}Ti_{2.23}O_{7.52}$ heated at 1400ºC in air.
U is assumed to be +4 in this sample.

Phase	Ca	Hf	Pu	U	Gd	Al	Ti	O	Total
Pyrochlore	0.98	0.28	0.26	0.42	0.21	0.07	1.85	7.00	11.07
Brannerite	0.10	0.13	0.26	0.47	0.14	0.09	1.92	6.00	9.11
PuO_2	0.11	0.06	0.43	0.36	0.07	0.06		2.00	3.09
Rutile		0.11		0.01		0.02	0.86	2.00	3.00

Table A132. Microprobe analysis of ME3688R.
Composition $Ca_{1.07}Hf_{0.26}Pu_{0.23}U_{0.35}Gd_{0.21}Ti_{2.25}O_{7.56}$ heated at 1350ºC in Ar.

Phase	Ca	Hf	Pu	U	Gd	Ga	Al	Ti	O	Total
Pyrochlore	1.163	0.245	0.219	0.413	0.178	0.003	0.001	1.778	6.746	10.746
Perovskite	0.887	0.012	0.008	0.003	0.057	0.002	0.008	1.023	3.080	5.080

Table A133. Quantitative SEM/EDS analysis of R97m030 (1325ºC Wet Mill-Ar) [11].
Composition $Ca_{0.89}Hf_{0.26}Pu_{0.22}U_{0.44}Gd_{0.22}Ti_{2.23}O_{7.52}$ heated at 1325ºC in Ar.

Phase	Ca	Hf	Pu	U	Gd	Al	Ti	O	Total
Pyrochlore	0.93	0.28	0.24	0.41	0.20	0.05	1.92	7.00	11.03
Brannerite	0.11	0.12	0.19	0.57	0.11	0.07	1.92	6.00	9.09
PuO_2	0.08	0.04	0.34	0.53	0.08			2.00	3.07
Rutile		0.09		0.01			0.90	2.00	3.00

Table A134. Quantitative SEM/EDS analysis of R97m030 (1325ºC Dry Mill-Ar) [11].
Composition $Ca_{0.89}Hf_{0.26}Pu_{0.22}U_{0.44}Gd_{0.22}Ti_{2.23}O_{7.52}$ heated at 1325ºC in Ar.

Phase	Ca	Hf	Pu	U	Gd	Al	Ti	O	Total
Pyrochlore	0.91	0.27	0.23	0.44	0.20	0.08	1.91	7.00	11.04
Brannerite	0.07	0.13	0.22	0.59	0.13	0.07	1.88	6.00	9.09
PuO_2	0.08	0.05	0.32	0.53	0.08			2.00	3.06
Rutile		0.10		0.01			0.89	2.00	3.00

Table A135. Quantitative SEM/EDS analysis of R97m030 (1350ºC Wet Mill-Ar) [11].
Composition $Ca_{0.89}Hf_{0.26}Pu_{0.22}U_{0.44}Gd_{0.22}Ti_{2.23}O_{7.52}$ heated at 1350ºC in Ar.

Phase	Ca	Hf	Pu	U	Gd	Al	Ti	O	Total
Pyrochlore	0.91	0.26	0.26	0.44	0.21	0.05	1.89	7.00	11.02
Brannerite	0.05	0.14	0.19	0.56	0.11	0.06	1.95	6.00	9.06
PuO_2	0.07	0.03	0.29	0.54	0.06	0.04	0.03	2.00	3.06
Rutile		0.09		0.01		0.01	0.89	2.00	3.00

Table A136. Quantitative SEM/EDS analysis of R97m030 (1350ºC Dry Mill-Ar) [11].
Composition $Ca_{0.89}Hf_{0.26}Pu_{0.22}U_{0.44}Gd_{0.22}Ti_{2.23}O_{7.52}$ heated at 1350ºC in Ar.

Phase	Ca	Hf	Pu	U	Gd	Al	Ti	O	Total
Pyrochlore	0.90	0.26	0.26	0.43	0.19	0.03	1.94	7.00	11.01
Brannerite	0.05	0.15	0.23	0.60	0.09	0.05	1.90	6.00	9.07
PuO_2	0.06	0.03	0.50	0.40	0.03	0.02		2.00	3.04
Rutile		0.10		0.01			0.89	2.00	3.00

Table A137. Quantitative SEM/EDS analysis of R97m030 (1375ºC Wet Mill-Ar) [11].
Composition $Ca_{0.89}Hf_{0.26}Pu_{0.22}U_{0.44}Gd_{0.22}Ti_{2.23}O_{7.52}$ heated at 1375ºC in Ar.

Phase	Ca	Hf	Pu	U	Gd	Al	Ti	O	Total
Pyrochlore	0.92	0.26	0.27	0.41	0.22	0.02	1.92	7.00	11.02
Brannerite	0.07	0.14	0.19	0.57	0.12	0.03	1.96	6.00	9.08
PuO_2	0.07	0.03	0.36	0.49	0.04		0.06	2.00	3.04
Rutile		0.09		0.01			0.90	2.00	3.00

Table A138. Quantitative SEM/EDS analysis of R97m030 (1375ºC Dry Mill-Ar) [11].
Composition $Ca_{0.89}Hf_{0.26}Pu_{0.22}U_{0.44}Gd_{0.22}Ti_{2.23}O_{7.52}$ heated at 1375ºC in Ar.

Phase	Ca	Hf	Pu	U	Gd	Al	Ti	O	Total
Pyrochlore	0.87	0.29	0.27	0.43	0.19	0.11	1.86	7.00	11.02
Brannerite	0.06	0.16	0.18	0.61	0.09	0.12	1.87	6.00	9.09
PuO_2	0.03	0.03	0.40	0.46	0.04	0.08		2.00	3.04
Rutile		0.10		0.01		0.03	0.87	2.00	3.01

Table A138. Quantitative SEM/EDS analysis of R97m030 (1400ºC Wet Mill-Ar) [11].

Composition $Ca_{0.89}Hf_{0.26}Pu_{0.22}U_{0.44}Gd_{0.22}Ti_{2.23}O_{7.52}$ heated at 1400ºC in Ar.

Phase	Ca	Hf	Pu	U	Gd	Al	Ti	O	Total
Pyrochlore	0.87	0.26	0.24	0.41	0.22	0.09	1.91	7.00	11.00
Brannerite	0.05	0.15	0.23	0.54	0.11	0.12	1.89	6.00	9.09
PuO_2	0.06	0.03	0.31	0.50	0.04	0.07	0.06	2.00	3.07
Rutile		0.09		0.01		0.02	0.89	2.00	3.01

Table A139. Quantitative SEM/EDS analysis of R97m030 (1400ºC Dry Mill-Ar) [11].

Composition $Ca_{0.89}Hf_{0.26}Pu_{0.22}U_{0.44}Gd_{0.22}Ti_{2.23}O_{7.52}$ heated at 1400ºC in Ar.

Phase	Ca	Hf	Pu	U	Gd	Al	Ti	O	Total
Pyrochlore	0.87	0.28	0.28	0.42	0.22	0.05	1.89	7.00	11.01
Brannerite	0.05	0.14	0.20	0.58	0.09	0.06	1.94	6.00	9.06
PuO_2	0.04	0.03	0.47	0.41	0.05	0.05		2.00	3.05
Rutile		0.09		0.01		0.01	0.88	2.00	2.99

Table A140. Quantitative SEM/EDS analysis of Pu67 [18].

Composition $Ca_{0.89}Hf_{0.25}Pu_{0.22}U_{0.44}Gd_{0.22}Ti_{2.25}O_{7.55}$ heated at 1350ºC in Ar.

Phase	Ca	Hf	Pu	U	Gd	Al	Ti	O	Total
Pyrochlore	0.90	0.26	0.26	0.43	0.19	0.03	1.94	7.00	11.01
Brannerite	0.05	0.15	0.23	0.60	0.09	0.05	1.90	6.00	9.09
PuO_2	0.06	0.03	0.50	0.40	0.03	0.02		2.00	3.04
Rutile		0.10		0.01			0.89	2.00	3.00

Table A141. Quantitative SEM/EDS analysis of Pu68 [18].

Composition $Ca_{0.89}Hf_{0.25}Pu_{0.22}U_{0.44}Gd_{0.22}Ti_{2.25}O_{7.55}$ heated at 1350ºC in Ar.

Phase	Ca	Hf	Pu	U	Gd	Ti	O	Total
Pyrochlore	0.99	0.22	0.21	0.41	0.24	1.98	7.00	11.05
Brannerite	0.08	0.11	0.21	0.53	0.14	2.00	6.00	9.08
PuO_2	0.11	0.03	0.40	0.42	0.08	0.04	2.00	3.07
Rutile	0.001	0.08	0.001	0.009	0.002	0.91	2.00	3.00

Table A142. Quantitative SEM/EDS analysis of mws980293 [18].

Composition $Ca_{0.89}Hf_{0.25}Pu_{0.22}U_{0.44}Gd_{0.22}Ti_{2.25}O_{7.55}$ heated at 1350ºC in Ar.

Phase	Ca	Hf	Pu	U	Gd	Ti	O	Total
Pyrochlore	1.01	0.23	0.22	0.42	0.23	1.96	7.00	11.07
Brannerite	0.09	0.12	0.21	0.53	0.13	1.99	6.00	9.07
Rutile	0.001	0.08	0.002	0.007		0.91	2.00	3.00

Table A143. Quantitative SEM/EDS analysis of mws980294 [18].

Composition $Ca_{0.89}Hf_{0.62}Pu_{0.19}U_{0.31}Gd_{0.20}Al_{0.12}Ti_{2.29}O_{8.01}$ heated at 1350ºC in Ar.

Phase	Ca	Hf	Pu	U	Gd	Al	Ti	O	Total
Pyrochlore	0.99	0.27	0.25	0.37	0.23		1.94	7.00	11.05
zirconolite-2M	0.82	0.75	0.08	0.11	0.16	0.24	1.86	7.00	11.01
Brannerite	0.08	0.13	0.25	0.50	0.12		1.99	6.00	9.07
Rutile	0.002	0.10	0.001	0.009		0.01	0.85	2.00	3.00

Table A144. Quantitative SEM/EDS analysis of mws980295 [18].

Composition $Ca_{0.51}Hf_{0.23}Pu_{0.23}U_{0.50}Gd_{0.17}Ti_{2.25}O_{6.95}$ heated at 1350ºC in Ar.

Phase	Ca	Hf	Pu	U	Gd	Ti	O	Total
Pyrochlore	1.06	0.22	0.22	0.47	0.24	1.89	7.00	11.09
Brannerite	0.10	0.11	0.19	0.52	0.15	2.02	6.00	9.09
PuO_2	0.14	0.07	0.28	0.49	0.11	0.006	2.00	3.10

Table A145. Quantitative SEM/EDS analysis of mws980352 [18].

Composition $Ca_{0.89}Hf_{0.62}Pu_{0.19}U_{0.31}Gd_{0.20}Al_{0.12}Ti_{2.29}O_{8.01}$ heated at 1350ºC in Ar.

Phase	Ca	Hf	Pu	U	Gd	Al	Ti	O	Total
Pyrochlore	0.95	0.28	0.28	0.36	0.22		1.94	7.00	11.03
Zirconolite-2M	0.83	0.76	0.08	0.10	0.15	0.20	1.89	7.00	11.00
Brannerite	0.05	0.15	0.27	0.47	0.13	0.04	1.97	6.00	9.07
PuO_2		0.004	0.91	0.014			0.07	2.00	3.00
Rutile		0.11	0.001	0.008		0.01	0.88	2.00	3.00

Table A146. Quantitative SEM/EDS analysis of mws980353 [18].

Composition $Ca_{0.89}Hf_{0.62}Pu_{0.19}U_{0.31}Gd_{0.20}Al_{0.12}Ti_{2.29}O_{8.01}$ heated at 1350ºC in Ar.

Phase	Ca	Hf	Pu	U	Gd	Al	Ti	O	Total
Pyrochlore	0.94	0.29	0.27	0.37	0.24		1.93	7.00	11.03
zirconolite-2M	0.83	0.77	0.07	0.10	0.14	0.23	1.86	7.00	11.00
Brannerite	0.06	0.13	0.33	0.43	0.14	0.04	1.95	6.00	9.07
PuO_2		0.004	0.95	0.009			0.04	2.00	3.00
Rutile		0.11	0.007	0.008		0.01	0.88	2.00	3.00

Table A147. Quantitative SEM/EDS analysis of mws980354 [18].

Composition $Ca_{0.51}Hf_{0.23}Pu_{0.23}U_{0.50}Gd_{0.17}Ti_{2.25}O_{6.95}$ heated at 1350ºC in Ar.

Phase	Ca	Hf	Pu	U	Gd	Ti	O	Total
Pyrochlore	0.97	0.25	0.24	0.41	0.22	1.96	7.00	11.04
Brannerite	0.07	0.13	0.22	0.51	0.12	2.01	6.00	9.06
Rutile		0.09		0.006		0.90	2.00	3.00

Table A148. Quantitative SEM/EDS analysis of mws980355 [18].

Composition $Ca_{0.51}Hf_{0.23}Pu_{0.23}U_{0.50}Gd_{0.17}Ti_{2.25}O_{6.95}$ heated at 1350°C in Ar.

Phase	Ca	Hf	Pu	U	Gd	Ti	O	Total
Pyrochlore	0.95	0.27	0.24	0.40	0.22	1.94	7.00	11.04
Brannerite	0.07	0.14	0.23	0.51	0.13	1.99	6.00	9.07
PuO_2		0.003	0.95	0.006		0.04	2.00	3.00
Rutile		0.10	0.001	0.006		0.89	2.00	3.00

Table A149. Quantitative SEM/EDS analysis of mws980356 [18].

Composition $Ca_{1.07}Hf_{0.26}Pu_{0.23}U_{0.35}Gd_{0.21}Ti_{2.25}O_{7.56}$ heated at 1350°C in Ar.

Phase	Ca	Hf	Pu	U	Gd	Ti	O	Total
Pyrochlore	1.03	0.22	0.23	0.35	0.20	2.04	7.00	11.07
Rutile	0.004	0.06	0.001	0.004		0.94	2.00	3.00

Table A150. Quantitiative SEM/EDS analysis of mws980357 [18].

Composition $Ca_{1.07}Hf_{0.26}Pu_{0.23}U_{0.35}Gd_{0.21}Ti_{2.25}O_{7.56}$ heated at 1350°C in Ar.

Phase	Ca	Hf	Pu	U	Gd	Ti	O	Total
Pyrochlore	0.99	0.22	0.24	0.37	0.21	2.01	7.00	11.05
PuO_2			1.00				2.00	3.00
Rutile	0.003	0.06	0.001	0.004		0.93	2.00	3.00

Table A151. Quantitative SEM/EDS analysis of mws980361 [18].

Composition $Ca_{1.07}Hf_{0.26}Pu_{0.23}U_{0.35}Gd_{0.21}Ti_{2.25}O_{7.56}$ heated at 1350°C in Ar.

Phase	Ca	Hf	Pu	U	Gd	Ti	O	Total
Pyrochlore	1.00	0.21	0.21	0.37	0.21	2.05	7.00	11.05
Rutile	0.002	0.06		0.01		0.93	2.00	3.00